



## Article

# Green Biofabrication of Silver Nanoparticles of Potential Synergistic Activity with Antibacterial and Antifungal Agents against Some Nosocomial Pathogens

Fatimah O. Al-Otibi, Mohamed Taha Yassin \* , Abdulaziz A. Al-Askar and Khalid Maniah

Botany and Microbiology Department, College of Science, King Saud University, Riyadh 11451, Saudi Arabia

\* Correspondence: myassin2.c@ksu.edu.sa

**Abstract:** Nosocomial bacterial and fungal infections are one of the main causes of high morbidity and mortality worldwide, owing to the high prevalence of multidrug-resistant microbial strains. Hence, the study aims to synthesize, characterize, and investigate the antifungal and antibacterial activity of silver nanoparticles (AgNPs) fabricated using *Camellia sinensis* leaves against nosocomial pathogens. The biogenic AgNPs revealed a small particle diameter of  $35.761 \pm 3.18$  nm based on transmission electron microscope (TEM) graphs and a negative surface charge of  $-14.1$  mV, revealing the repulsive forces between nanoparticles, which in turn indicated their colloidal stability. The disk diffusion assay confirmed that *Escherichia coli* was the most susceptible bacterial strain to the biogenic AgNPs (200 g/disk), while the lowest sensitive strain was found to be the *Acinetobacter baumannii* strain with relative inhibition zones of  $36.14 \pm 0.67$  and  $21.04 \pm 0.19$  mm, respectively. On the other hand, the biogenic AgNPs (200  $\mu$ g/disk) exposed antifungal efficacy against *Candida albicans* strain with a relative inhibition zone of  $18.16 \pm 0.14$  mm in diameter. The biogenic AgNPs exposed synergistic activity with both tigecycline and clotrimazole against *A. baumannii* and *C. albicans*, respectively. In conclusion, the biogenic AgNPs demonstrated distinct physicochemical properties and potential synergistic bioactivity with tigecycline, linezolid, and clotrimazole against gram-negative, gram-positive, and fungal strains, respectively. This is paving the way for the development of effective antimicrobial combinations for the effective management of nosocomial pathogens in intensive care units (ICUs) and health care settings.

**Keywords:** green synthesis; *Camellia sinensis*; silver nanomaterials; antimicrobial; synergism



**Citation:** Al-Otibi, F.O.; Yassin, M.T.; Al-Askar, A.A.; Maniah, K. Green Biofabrication of Silver Nanoparticles of Potential Synergistic Activity with Antibacterial and Antifungal Agents against Some Nosocomial Pathogens.

*Microorganisms* **2023**, *11*, 945.

<https://doi.org/10.3390/microorganisms11040945>

Academic Editors: Wajid Zaman and Hakim Manghwar

Received: 2 March 2023

Revised: 20 March 2023

Accepted: 21 March 2023

Published: 4 April 2023



**Copyright:** © 2023 by the authors. Licensee MDPI, Basel, Switzerland. This article is an open access article distributed under the terms and conditions of the Creative Commons Attribution (CC BY) license (<https://creativecommons.org/licenses/by/4.0/>).

## 1. Introduction

Nosocomial microbial infections represent a public health burden worldwide, contributing to a high number of morbidities and fatalities every year [1]. These infections refer to illnesses that have occurred among hospitalized patients and are the result of various toxins or infectious agents [2]. There is a wide range of variance in the rates of occurrence of nosocomial infections across different geographical areas and during different periods of time [3]. Nosocomial bloodstream infection (NBSI), nosocomial pneumonia infection (NPNEU), nosocomial surgical site infection (SSI), and nosocomial urinary tract infection (UTI) account for 80% of all nosocomial infections [4]. The main cause behind the incidence of nosocomial infections is drug-resistant strains [5]. In developing and developed countries, it is projected that 10 and 7 patients out of every 100 inpatients in healthcare facilities may become infected with hospital-acquired illnesses, respectively [6]. In this context, several microbial strains, including methicillin-resistant *Staphylococcus aureus* [7], *Escherichia coli* [8], *Acinetobacter baumannii* [9], and *Candida albicans* [10], have been reported to cause hospital-acquired infections. Due to their role in a number of infectious diseases that can be fatal, multidrug-resistant bacteria pose a severe threat to public health globally [11]. Pollution, mutation, changing environmental circumstances, and excessive drug

usage all contribute to the ongoing rise in multidrug-resistant bacterial species [12,13]. To solve this issue, researchers are working to create novel medications for the treatment of these microbial illnesses [14].

Nanotechnology provides a distinct platform for the modification and production of unique metal features ranging in size from 1–100 nm with potential applications in cell labeling, diagnostics, biomarkers, pharmaceuticals, mechanics, optics, agriculture, electronics, biomedicine, and antimicrobial applications [15–18]. The AgNPs have a large surface area and small particle size, which allows for extensive contact with microorganisms [19,20]. These characteristics of AgNPs significantly enhance their biological and chemical capabilities, which notably aid in their demonstration as potent bactericidal compounds [21]. Nanometals were distinguished by their oligodynamic impact, which was the microbicidal action of metals, particularly heavy metals, at low concentrations [22]. In this respect, silver is one of the oligodynamic materials that has received a lot of attention because of its low toxicity, high efficacy, and broad variety of disinfection uses [23]. The high surface area of AgNPs is the major distinguishing feature of oligodynamic materials, enabling them to bind effectively to bacterial cells, penetrating them, and producing free radicals and reactive oxygen species [24]. Briefly, AgNPs have four recognized antibacterial effects: (1) adherence to the microbial membrane's surface; (2) when AgNPs enter cells, they disrupt biomolecules and cause intracellular damage; (3) they cause cellular toxicity by producing ROS that create oxidative stress in the cell; and (4) they interfere with the cell's signal transduction pathways [25].

The green synthesis of AgNPs via biological methods offers numerous benefits over physical and chemical synthesis since these methods use hazardous materials, have high equipment costs, and generate toxic compounds, while biological synthesis is simple, inexpensive, non-toxic, and environmentally friendly [26]. Due to the availability of several plants and their straightforward and secure application, plant-mediated synthesis of AgNPs is an extensively used approach for the biofabrication of AgNPs [27,28]. The facile bioformulation of silver nanomaterials is mediated by the presence of many phytochemical ingredients in plant extracts, such as flavonoids, phenols, tannins, polysaccharides, amino acids, terpenoids, and proteins [29]. For instance, the aqueous extracts of *Zataria multiflora*, *Ctenolepis garcini* leaves, and *Moringa oleifera* seeds mediated the green bioformulation of AgNPs against different bacterial strains such as *S. aureus*, *Pseudomonas aeruginosa*, *E. coli*, and *Salmonella typhi*, recording inhibitory zones ranging from 14 to 28.5 mm [30–32]. Recent research found that biogenic AgNPs had synergistic action with fluconazole and metronidazole antifungals against *C. albicans*, as well as synergistic activity with ciprofloxacin, cefixime, and bacitracin antibiotics against *P. aeruginosa* strains [33]. Several reports investigated the synergistic potency of AgNPs with antibiotics such as streptomycin, amikacin, ampicillin, and polymyxin B against *E. coli*, *S. aureus*, and *A. baumannii* [34–36].

Green tea extract contains a high level of polyphenolic compounds such as catechol, caffeine, 1,2,3-benzenetriol, 1,3,5-benzenetriol, and methoxy resorcinol, indicating the possibility of production of AgNPs utilizing this extract since phenolic components are significant in metal reduction [37]. Previous research detailed the green synthesis of AgNPs using green tea extract and proved the antibacterial activity of the biogenic AgNPs against *Klebsiella* spp. and *S. aureus* at doses ranging from 5 to 20 mg/mL [38]. Another study used green tea extract to create AgNPs and showed antibacterial efficacy against *E. coli* and *S. aureus*, with inhibition zones of 16 and 14 mm, respectively [39]. Previous studies have confirmed the possible biosynthesis of AgNPs using green tea extract due to its high polyphenolic component and antioxidant content; however, none of the prior studies have looked into the synergistic patterns of AgNPs with antibacterial and antifungal drugs. As a result, the present study was designed to evaluate the synergistic effects of AgNPs produced utilizing green tea extract with antimicrobial drugs against some nosocomial bacterial and fungal strains.

## 2. Materials and Methods

### 2.1. Preparation of Green Tea Leaves Extract

The Chinese green tea, namely *Camellia sinensis* var. *sinensis*, which is characterized by its small leaves, was obtained from a local market in Saudi Arabia. The plant materials were identified by the Botany and Microbiology Department's Herbarium Staff and deposited in the herbarium with voucher number KSU-23592. For the preparation of the water extract of *C. sinensis* leaves, the leaves were first washed with running tap water, then rinsed in distilled water, and then dried completely. Afterward, the dried leaves were blended using a mechanical mortar to obtain the homogenous powder, and then 50 g of the powdered leaves were placed in an Elementer flask (500 mL) for submerging in 200 mL distilled water under heating at 70 °C for half an hour. The aqueous extract of green tea leaves was incubated over a magnetic stirrer for 24 h at 25 °C, then filtered using Whatman filter paper (1) to get rid of any impurities [40–42]. Preservation of the extract in the refrigerator was conducted for subsequent AgNP synthesis.

### 2.2. Green Biofabrication of AgNPs

The leaf water extract of *C. sinensis* was utilized as a reducing agent for the formulation of AgNPs using silver nitrate solution. The salt of AgNO<sub>3</sub> was purchased from Sigma-Aldrich, Saint Louis, MO, USA. Ten milliliters of the green tea extract were added to 90 mL of AgNO<sub>3</sub> solution (1 mM) and then incubated in a shaking incubator under dark conditions for 24 h at 25 °C. The visual observation of the color change of the colorless silver nitrate solution to dark brown following incubation with green tea extract initially verified the formation of AgNPs. For harvesting the biogenic AgNPs, the reaction mixture was centrifuged at 10,000 rpm for 10 min, and the supernatant was discarded. The collected precipitate was washed thrice with distilled water for removal of any remaining extract, then incubated at 80 °C for complete drying and subsequent analytical characterization.

### 2.3. Physicochemical Characterization of Biogenic AgNPs

The optical absorption of the biogenic AgNPs was conducted using a UV-Vis spectrophotometer (UV-1601, Shimadzu, Kyoto, Japan), while Fourier transform infrared spectroscopy (FTIR) measurements were performed to investigate the interaction between plant metabolites and the biosynthesized AgNPs. In addition, the morphological features of the biogenic AgNPs were studied using transmission electron microscope (JEOL, JEM1011, Tokyo, Japan) analysis for the investigation of particle shape, size, and distribution. The elemental pattern of the biogenic AgNPs was examined using energy dispersive X-ray (EDX) analysis (JEOL, JSM-6380 LA, Tokyo, Japan). Moreover, the crystallographic characteristics were studied using X-ray powder diffraction (XRD) examination (Shimadzu, Columbia, MD, USA), whereas the surface charge and hydrodynamic diameter of the fabricated AgNPs were detected using a Zeta sizer instrument (Malvern Instruments Ltd.; zs90, Worcestershire, UK) [43,44].

### 2.4. Antimicrobial Potency of Biogenic AgNPs against Different Microbial Strains

Four nosocomial microbial strains were investigated for their susceptibility to the biogenic AgNPs, namely *C. albicans* (ATCC 18804), MRSA (ATCC 33592), *A. baumannii* (ATCC 43498), and *E. coli* (ATCC 25922). The microbial suspension was prepared using sterile saline solution (0.85%) by picking up the colonies of 24 h cultures and dipping them into the saline solution [40,41]. The turbidity of the microbial suspension was adjusted using 0.5 McFarland standard to achieve viable bacterial and fungal cell counts of  $1.0 \times 10^8$  and  $1.0 \times 10^6$  cfu/mL, respectively. The prepared microbial suspensions (0.5 mL) were pipetted and spread over freshly prepared Mueller–Hinton agar (MHA) medium. Tigecycline and clotrimazole, as standard antibacterial and antifungal agents, respectively, were purchased from Sigma–Aldrich (St. Louis, MO, USA). The antimicrobial agents were solubilized in methanol and sonicated to ensure complete solubilization, then sterile filter paper disks were impregnated with tigecycline and clotrimazole as antibacterial and antifungal positive

controls to achieve final concentrations of 15 and 10 µg/disk, respectively. In addition, sterile filter paper disks (8 mm in diameter) were loaded with 200 µg of AgNPs after their solubilization in methanol, while filter paper disks filled with methanol only were used as negative controls. Finally, the loaded disks were placed over the seeded layer and then preserved for 4 h in the refrigerator to allow AgNPs diffusion. The inhibition zones were measured using a Vernier caliper after a 24-h incubation period at 35 °C. The minimum inhibitory concentration of biogenic AgNPs generated from *C. sinensis* leaf extract was determined using a broth microdilution assay in 96-well microtitre plates against *E. coli* and *C. albicans* strains [45,46]. In addition, the minimum bactericidal (MBC) and fungicidal (MFC) concentrations were evaluated by culturing inoculums from MIC wells over freshly prepared MHA plates, incubating them at 35 °C overnight, and finally examining the plates for bacterial and fungal growth. The lowest concentrations of AgNPs that showed no bacterial or fungal growth were registered as MBC and MFC, respectively.

### 2.5. Investigation of the Ultrastructural Changes of Microbial Cells Treated with AgNPs Using SEM Analysis

The deformations caused by the biogenic AgNPs against MRSA, a gram-positive strain; *E. coli*, a gram-negative strain; and also against the fungal strain, *C. albicans*, were observed by scanning electron microscopy (SEM) examination. Agar pieces were taken from the inhibition zones and preserved in 3% (*v/v*) glutaraldehyde for 1 h at 25 °C (buffered with 0.1 M sodium phosphate buffer, pH 7.2). The fixed agar pieces were then washed four times in buffer. The pieces were washed four times in buffer after being post-fixed in 1% (*w/v*) osmium tetroxide (OsO<sub>4</sub>) for 1 h. The samples were then alcohol dehydrated for 15 min using a variety of ethanol strengths (30–100%). The samples were dried before being adhered to stubs using double-sided carbon tape. A Polaron SC 502 sputter coater was then used to deposit a thin layer of gold onto the specimens. Lastly, they were investigated using a scanning electron microscope (JEOL JSM-6380 LA).

### 2.6. Synergistic Antimicrobial Efficiency of Biogenic AgNPs with Antimicrobial Agents

The MIC concentration of biogenic AgNPs was tested for synergistic activity with tigecycline and clotrimazole antimicrobial agents against the tested bacterial and fungal pathogens using the standard disk diffusion assay [47]. In addition, the synergism of AgNPs with linezolid was also assessed against MRSA strain. For this, sterile filter paper disks were loaded with MIC and two-fold MIC concentrations of AgNPs, while another group of disks was impregnated with both AgNPs (40 µg/disk) and tigecycline (15 µg/disk). In addition, filter paper disks loaded with methanol were utilized as a negative control, whereas tigecycline disks were used as positive controls. Moreover, clotrimazole (10 µg/disk) and linezolid (30 µg/disk) disks were tested for synergism with AgNPs against *C. albicans* and MRSA strains, respectively. The impregnated disks were placed over the MHA plates seeded with microbial suspensions, as mentioned above. Finally, the plates were incubated at 35 °C overnight, and then inhibition zones were measured for determination of relative synergistic activity as demonstrated in the following equation:  $synergism \% = \frac{B-A}{A} \times 100$ , whereas A and B are the inhibition zones for the standard antimicrobial agent and antimicrobial agent+ AgNPs, respectively. The increase in fold of inhibition area (IFA) was calculated according to the following equation [48]:

$$(IFA) = (B^2 - A^2) / A^2$$

The fractional inhibitory concentration (FIC) index was calculated according to the following formula as presented in earlier studies [49,50].

FIC index (FICI) =  $\frac{\text{MIC of drug A in the combination}}{\text{MIC (A)}} + \frac{\text{MIC of drug B in the combination}}{\text{MIC (B)}}$ , whereas A referred to AgNPs and B referred to antibiotics.

The FICI detected as follows: FICI ≤ 0.5 synergistic effect, FICI = 0.5 to 1 additive effect, 2 ≤ FICI < 4 indifferent, and 4 < FICI antagonism.

## 2.7. Statistical Analysis

The data of current investigation was analyzed using GraphPad Prism version 8.0 (GraphPad Software, Inc., La Jolla, CA, USA) via one-way analysis of variance and Tukey's test. All experimentations were done in triplicates, and the data were presented as the mean of triplicates  $\pm$  standard error.

## 3. Results and Discussion

### 3.1. Green Biosynthesis of AgNPs

The primary indication of silver nanoparticle formation is the observed color change of the colorless silver nitrate solution after the addition of the plant extract. Figure 1A shows the colorless silver nitrate solution that, when reduced by green tea extract (Figure 1B), produced AgNPs with a dark brown color (Figure 1C). In this setting, the color change indicated the reduction of  $\text{Ag}^+$  ions through the action of plant metabolites leading to the formation of elemental nanosilver. Previous reports indicated that catechol, caffeine, 1,3,5-benzenetriol, 1,2,3-benzenetriol, and methoxy resorcinol, were the main phytoconstituents of aqueous leaf extract of *C. sinensis*, contributing to the reduction, stabilizing and capping of AgNPs (Figure 2) [51]. The detected UV peak at  $\lambda_{\text{max}}$  around 200 nm could be allocated to the adsorption of organic molecules on the AgNPs surface during the reduction process as phenolic acids, flavonoids, and heteroatoms such as S, O, N, and unsaturated groups [52]. The broad absorption peak noticed at 600 nm could be assigned to the surface plasmon resonance (SPR) of the biogenic AgNPs (Figure 3). The SPR peak of biogenic AgNPs has shifted to a longer wavelength at 600 nm due to the aggregation of AgNPs [53,54].

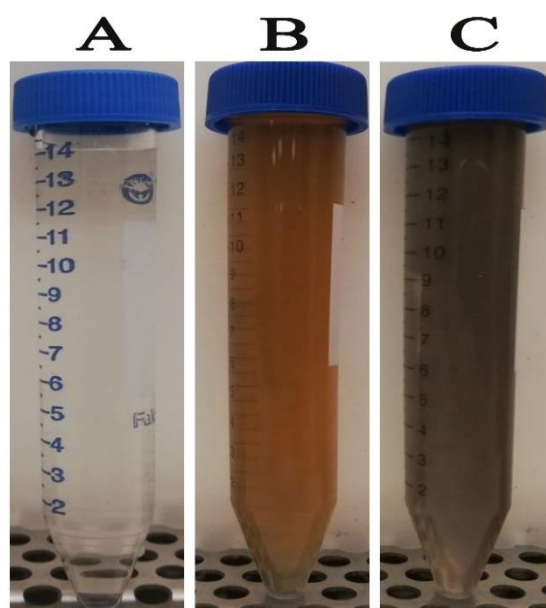


**Figure 1.** Green bioformulation of AgNPs using green tea extract. (A) refers to  $\text{AgNO}_3$  solution, (B) refers to water extract of green tea leaves, and (C) biogenic AgNPs.

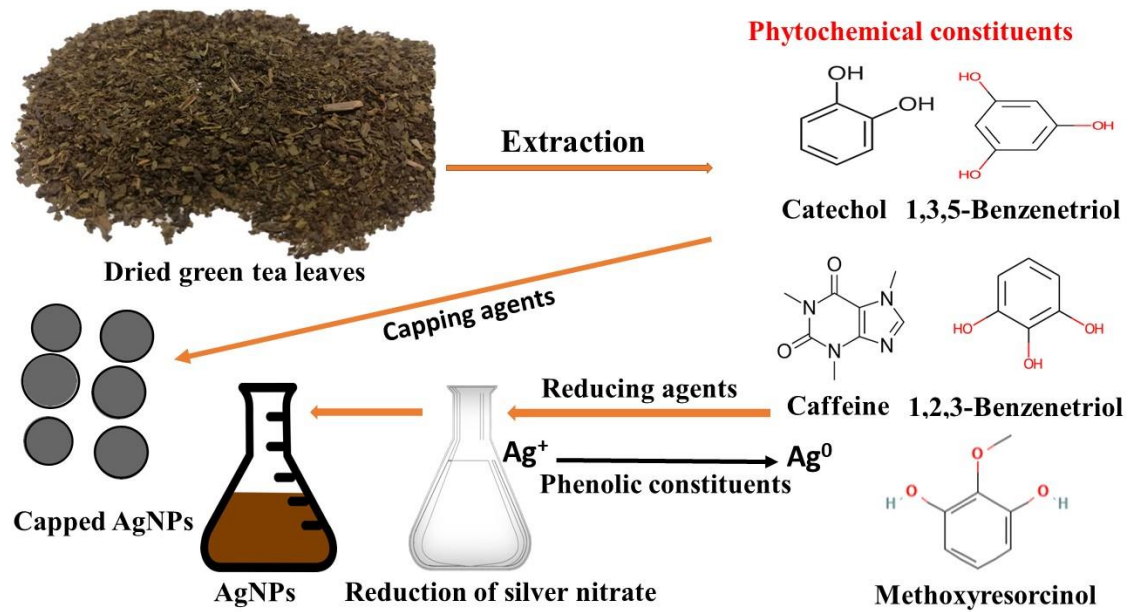


**Figure 2.** Schematic illustration of the green synthesis of biogenic silver nanoparticles (AgNPs) utilizing green tea leaves.

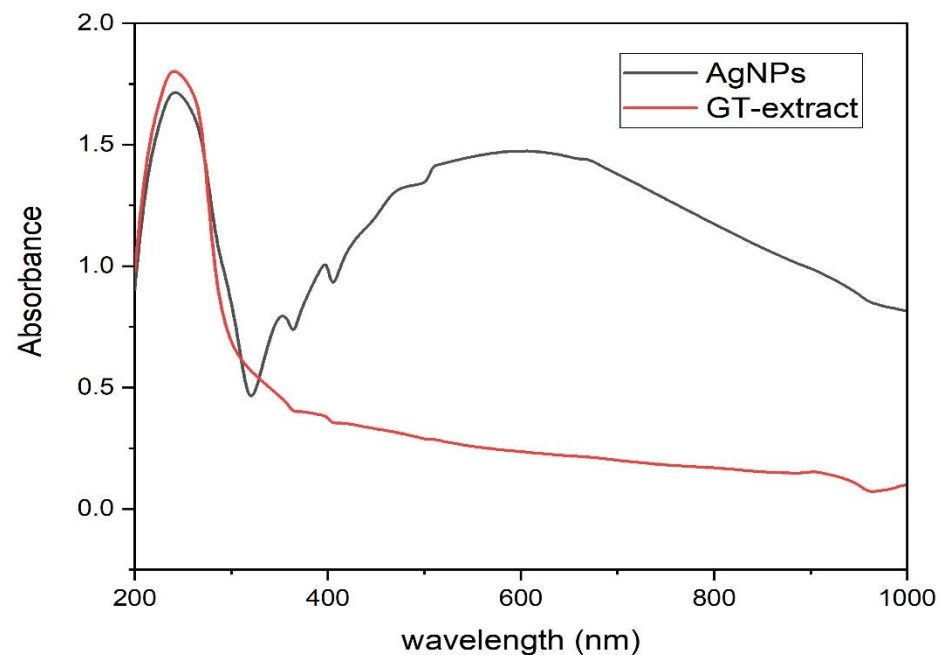


**Figure 3.** UV spectrum of the biogenic silver nanoparticles (AgNPs) and green tea (GT) water extract.

### 3.2. TEM Analysis of the Biofabricated AgNPs

The morphological features of the eco-friendly synthesized AgNPs of green tea extract were investigated using TEM analysis. TEM micrographs indicated that the biofabricated AgNPs were spherical in shape with the presence of capping biomolecules, as seen in Figure 4. The average particle size of the biosynthesized AgNPs was detected to be  $35.761 \pm 3.18$  nm, as demonstrated in Figure 5. Our findings were in accordance with those of a previous investigation, which indicated that the average particle size diameter of green tea-fabricated AgNPs was  $34.68 \pm 4.95$  nm [55].

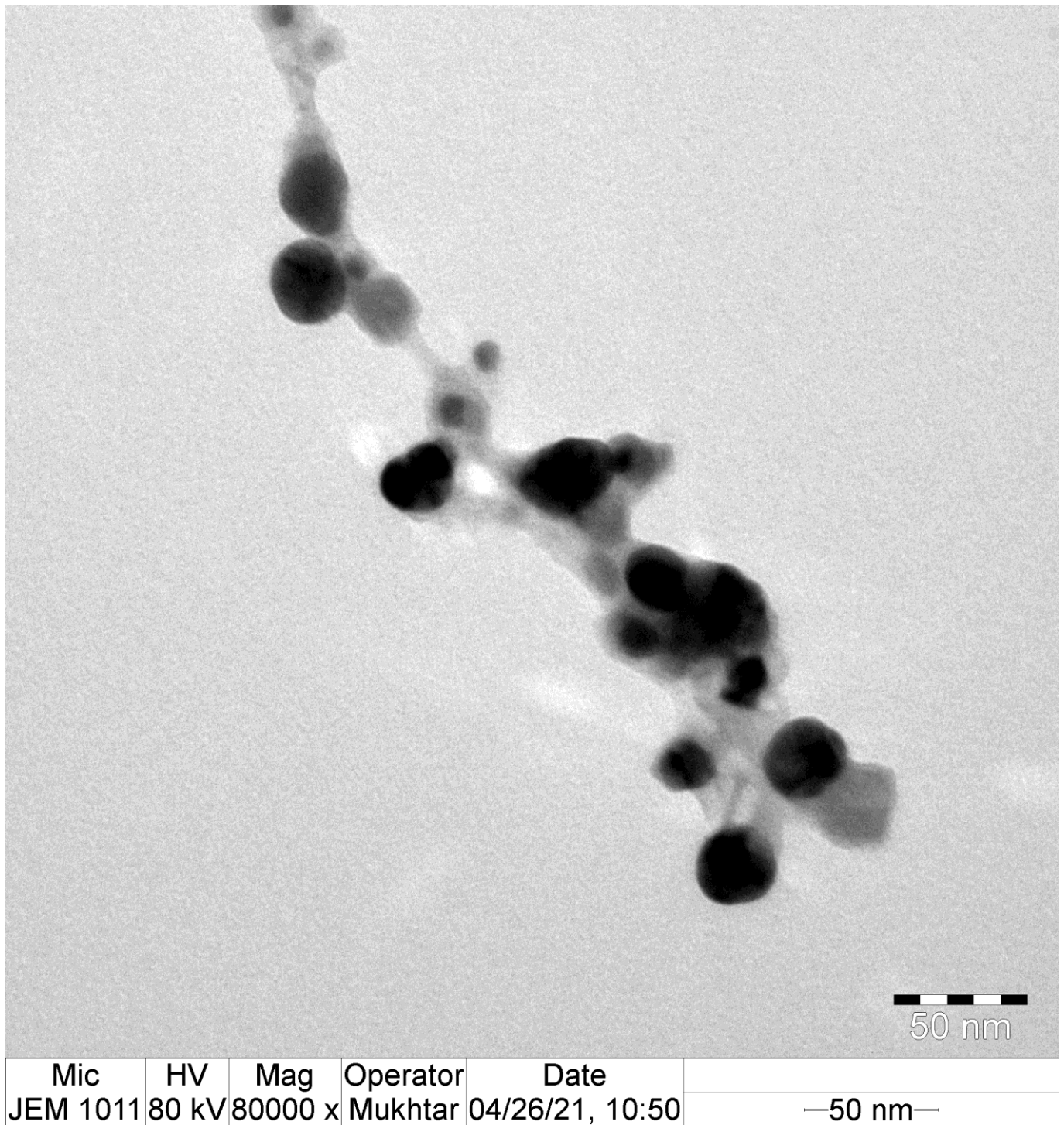


**Figure 4.** TEM micrograph of the eco-friendly synthesized AgNPs.

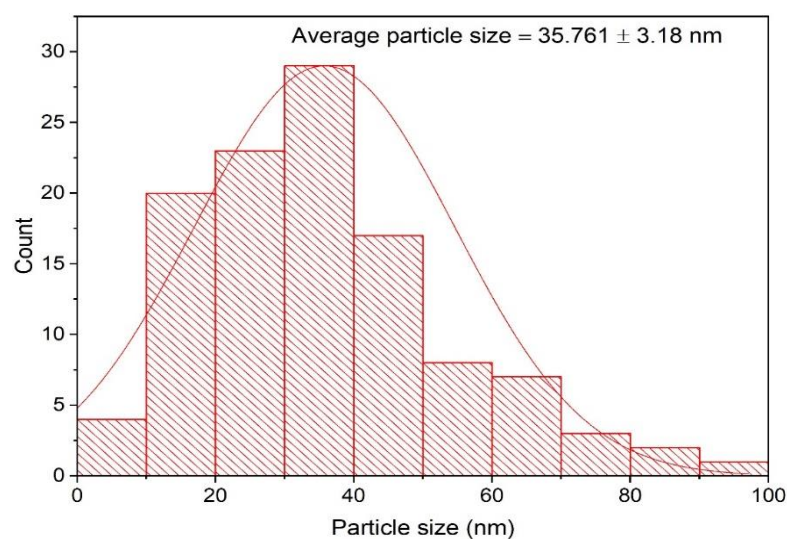


**Figure 5.** Particle size distribution histogram of the bioformulated AgNPs.

### 3.3. Elemental Investigation of the Biofabricated AgNPs

The elemental composition of the eco-friendly synthesized AgNPs was investigated utilizing energy-dispersive X-ray (EDX) analysis. EDX investigation indicated that the elemental mapping of the biogenic AgNPs was found to be composed of the following elements: silver, oxygen, carbon, and silicon Figure 6 [56]. The strong peak found at 2.983 keV was assigned to the elemental silver, indicating the successful biofabrication of AgNPs. In addition, the detected peak of elemental carbon was assigned to the carbon tape used for placing the biogenic AgNPs on the sample holder [57]. In addition, a previous investigation explained the presence of weak signals of other elements, such as silicon, in the EDX pattern and related this to the capping agents of the plant extracts adsorbed over the surface of AgNPs [58]. Additionally, the weak silicon peak might be attributable to X-ray emissions from carbohydrates or proteins in the extract [59].

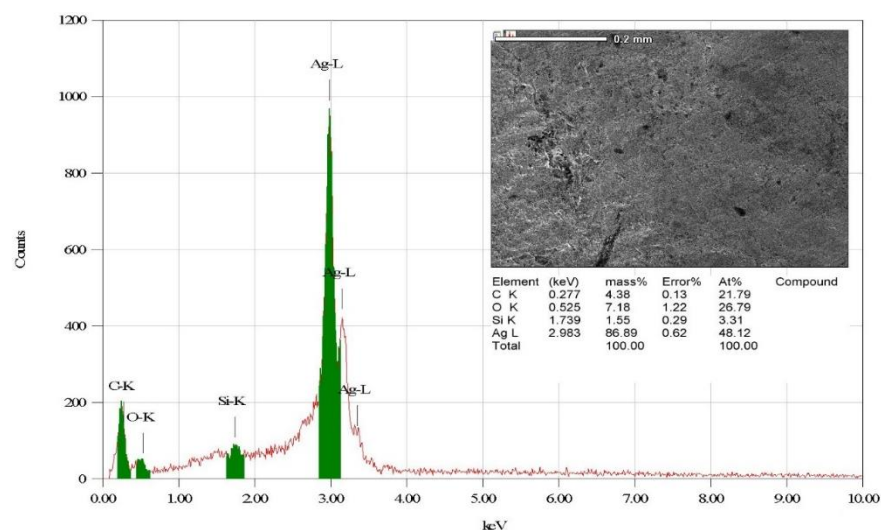


**Figure 6.** Elemental configuration of the bioformulated AgNPs.

### 3.4. Fourier Transform Infrared Spectroscopy (FT-IR) Investigation of AgNPs

FTIR analysis was used to investigate the bioformulated AgNPs and identify the key functional groups that led to their reduction, capping, and stabilization. In this context, the spectrum of FTIR investigation indicated the presence of five distinctive absorption bands, as seen in Figure 7. The strong band at  $3434.76\text{ cm}^{-1}$  was assigned to the O-H stretching of phenolic compounds in *C. sinensis* leaf extract, while the absorption band

noticed at  $2920.38\text{ cm}^{-1}$  was attributed to C–H stretching of aldehydes from plant metabolites (Table 1) [60,61]. In addition, the sharp peak at  $1631.37\text{ cm}^{-1}$  was clearly attributed to the C–O stretching or C–N bending of carboxylic compounds or amides, respectively [62]. Furthermore, the band noticed at  $1106.76\text{ cm}^{-1}$  could be assigned to the C–N stretching of aliphatic amines, which clarified the proteins of plant metabolites in the capping of the biosynthesized AgNPs, contributing to their stability and preventing their agglomeration [63]. The peak at  $584.97\text{ cm}^{-1}$  could be assigned to the Ag–O stretching, as reported in previous reports [64,65]. Together, the previous findings supported the notion that the functional groups of AgNPs, such as alcohols, phenols, aldehydes, carboxylic compounds, amides, and amines, helped reduce, stabilize, and cap the biofabricated AgNPs, thereby enhancing their stability and preventing agglomeration.

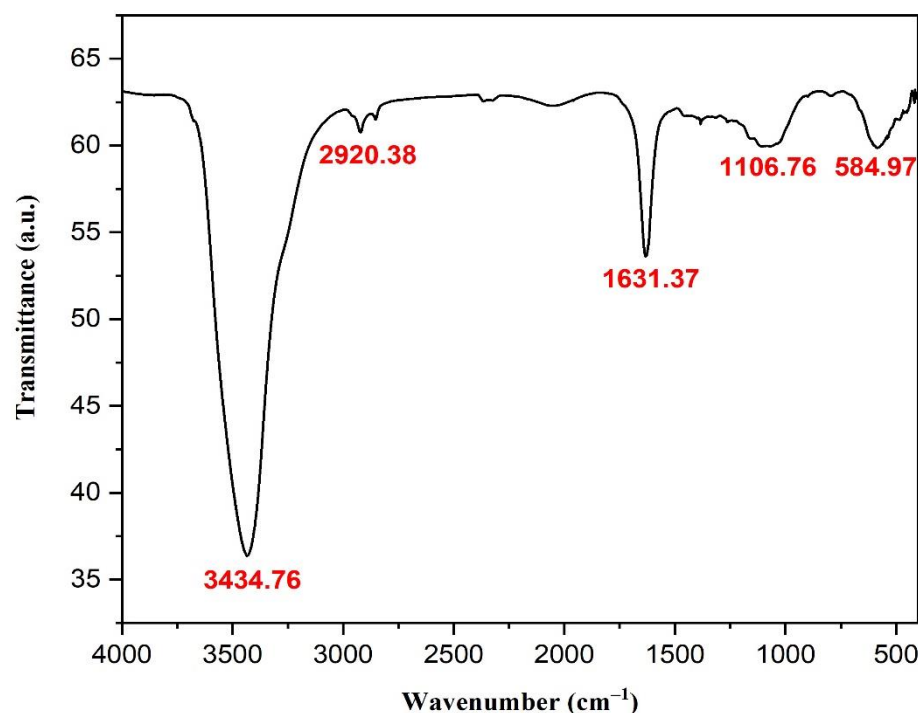


**Figure 7.** FTIR analysis of the biofabricated AgNPs.

**Table 1.** Functional groups of the biosynthesized AgNPs.

No.	Absorption Peak ( $\text{cm}^{-1}$ )	Appearance	Functional Groups	Molecular Motion
1	3434.76	Strong, broad	Alcohols and phenols	O–H stretching
2	2920.38	Weak	Aldehydes	C–H stretching
3	1631.37	Medium	Carboxylic compounds or amides	C–O stretching or C–N bending
4	1106.76	Weak, broad	Aliphatic amines	C–N stretching
5	584.97	Weak, broad	Metal oxygen bond	Ag–O stretching

### 3.5. X-ray Powder Diffraction (XRD) Analysis of the Biogenic AgNPs

The crystallographic properties of the biogenic AgNPs were studied using XRD analysis. In this setting, the XRD pattern revealed the presence of five sharp diffraction peaks at two theta ( $\theta$ ) angles of 32, 38, 44, 64, and  $77^\circ$ , which corresponded to the silver crystal planes of (110), (111), (200), (220), and (311) respectively, as shown in Figure 8. These findings affirmed the face-centered cubic (*fcc*) structure of the biosynthesized AgNPs as indicated by the Joint Committee on Powder Diffraction Standards (JCPDS), file no. 04-0783 [66]. Previous investigations documented the bioformulation of the *fcc* structure of crystalline

AgNPs formulated using different biogenic sources, such as *Euphrasia officinalis* leaf extract [67], tuber extract of *Arisaema flavum* [68], the leaf extract of *Holoptelea integrifolia* [69], and *Mangifera indica* leaf extract [70].

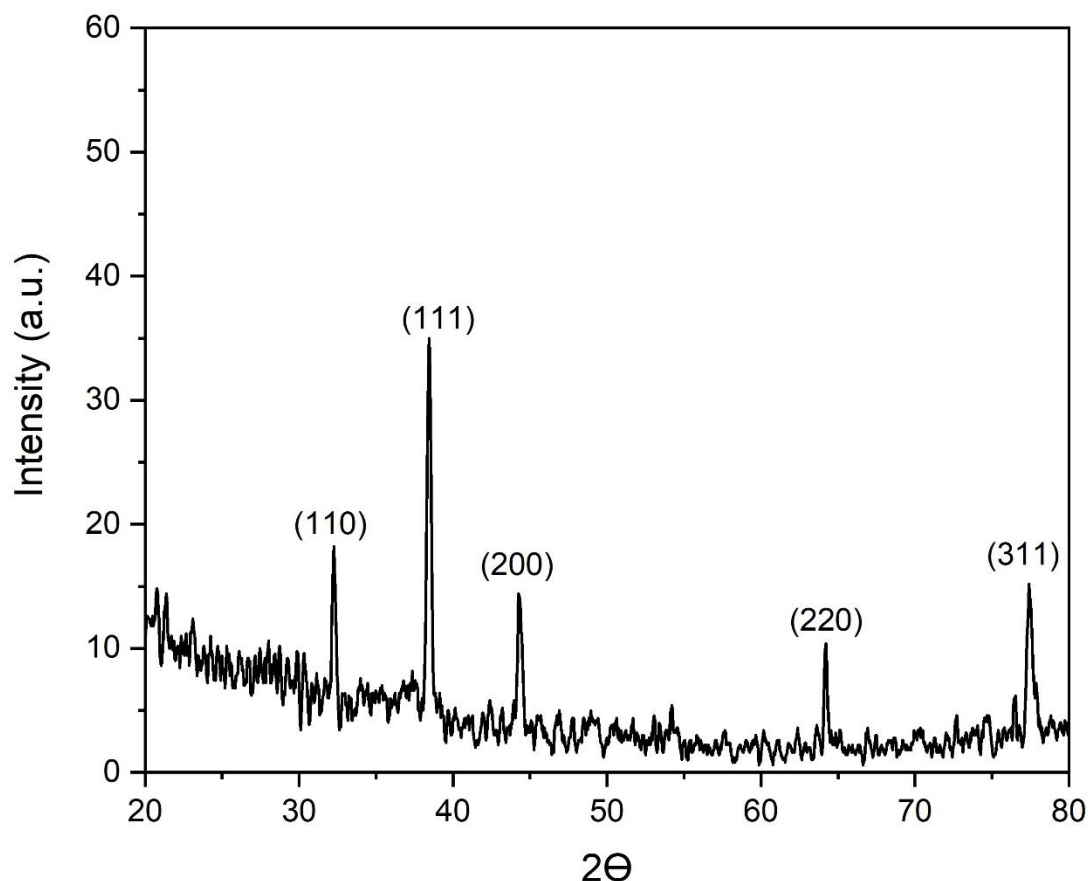


**Figure 8.** XRD pattern of silver nanoparticles formulated using green tea leaf extract.

### 3.6. Zeta Analysis of the Fabricated Silver Nanomaterials

The zeta potential is an important indicator of the stability of colloidal dispersion and also a sign of particle-related repulsion or attraction intensity [71]. Zeta potential analysis of the biofabricated AgNPs was conducted to detect the surface charge of the synthesized materials, which was found to be  $-14.1$  mV, as seen in Figure 9. Moreover, the estimated negative charge of the biogenic AgNPs provides colloidal stability owing to the mutual repulsion between the formulated nanomaterials [72]. Furthermore, the estimated negative charge of the synthesized AgNPs was in agreement with that of previous reports indicating the negative charge of biogenic silver nanomaterials synthesized using *Caesalpinia digyna* [73] and *Syzygium aromaticum* extracts [74]. The estimated negative charge on the surface of biogenic AgNPs could be assigned to the action of some capping molecules in green tea extract as the hydroxyl functional group of polyphenolic compounds [75]. On the other hand, the average hydrodynamic diameter of the synthesized nanomaterials was estimated utilizing the dynamic light scattering technique, as seen in Figure 10 [76]. In this context, the average hydrodynamic diameter was estimated to be 42.61 nm, which was slightly higher than that of TEM micrographs owing to the action of capping agents, which formed the core shell structure, in addition to the fact that the DLS technique estimated both the diameters of the nanoparticles and the adjacent hydrate layers [77,78]. The DLS pattern revealed the aggregation of AgNPs, revealing a wide peak in size, ranging from 100 to 1000 nm, which affirmed the action of capping molecules of the plant extract in acting as a shell for the nanoparticle aggregates. That explains the wide peak found in the DLS pattern and also the wide peak found in the UV spectrum around 600 nm [79]. The biogenic

AgNPs displayed a PDI value of 0.679, which indicated that the particles might aggregate with time [80].

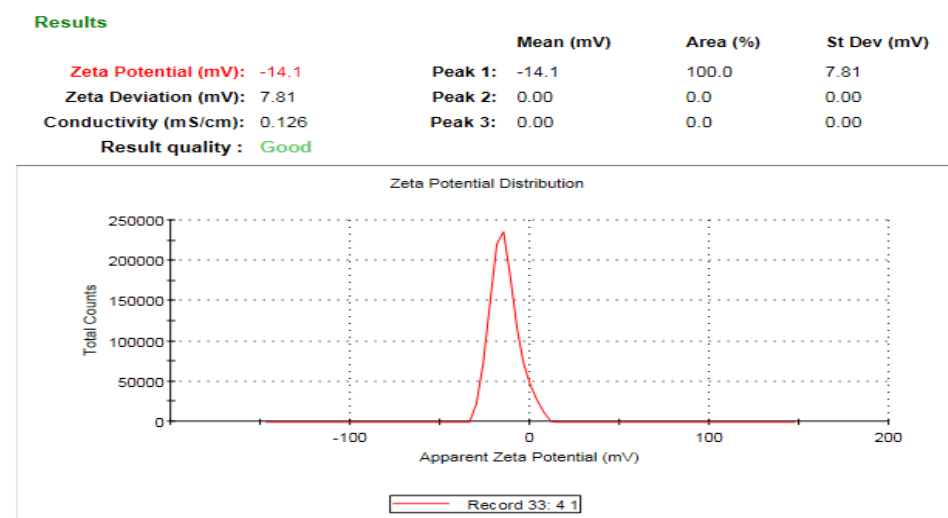


Figure 9. Surface charge of the biogenic silver nanomaterials.

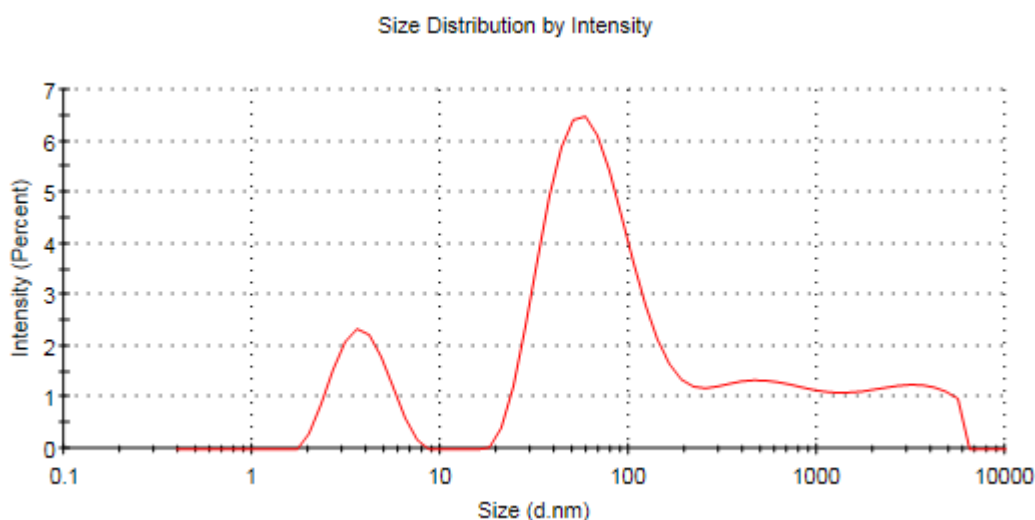


Figure 10. Dynamic light scattering pattern of the bioformulated AgNPs.

### 3.7. Screening of Antimicrobial Effectiveness of Biogenic AgNPs

The antibacterial effectiveness of the biogenic AgNPs was tested against MRSA, *E. coli*, *A. baumannii*, and *C. albicans* strains. The biofabricated AgNPs showed anticandidal efficacy against the *C. albicans* strain, with an average particle size diameter of  $18.16 \pm 0.14$  nm and a concentration of  $200 \mu\text{g}/\text{disk}$  (Table 2). Silver nanoparticles have remarkable anticandidal efficacy against *C. albicans* by damaging cell membranes and inhibiting normal cell division [81]. In addition, silver nanoparticles' anticandidal efficiency is caused by the creation of insoluble compounds containing sulfhydryl groups in candidal cell walls, as well as the breakdown of membrane-bound enzymes and lipids, which causes cell lysis [82]. Furthermore, the disruption of the candidal cell membrane and cell wall leads to the destabilization of membrane permeability, resulting in the leakage of potassium ions ( $\text{K}^+$ ) [83]. These events, triggered by the action of silver nanoparticles, resulting in the initiation of candidal cell death by disturbing cellular permeability, disrupting DNA replication, and inhibiting protein synthesis [84]. Excitingly, the biogenic AgNPs ( $200 \mu\text{g}/\text{disk}$ ) exposed antibacterial bioactivity against the tested bacterial strains, with inhibitory zones of  $28.17 \pm 0.21$ ,  $21.04 \pm 0.19$ , and  $36.14 \pm 0.67$  mm against MRSA, *A. baumannii*, and *E.*

*coli* strains, respectively. The antibacterial potency of the bioformulated AgNPs was significantly higher than that of the tigecycline control ( $p < 0.05$ ), whereas the bioactivity of these nanomaterials against *A. baumannii* strain was not significantly different ( $p > 0.05$ ) compared to control. In this context, the biosynthesized AgNPs have their antibacterial mode of action via a variety of pathways, including the continual discharge of silver ions ( $\text{Ag}^+$  ions), which is thought to be a microbe killing mechanism, or by the efficacy of AgNPs themselves [85]. The advantage of AgNPs over metallic silver or its salts is the regulated, steady release of  $\text{Ag}^+$  ions, which have a longer-lasting antibacterial impact [86]. Compared to antibiotics, microbes are considerably less likely to develop resistance to AgNPs [87]. The antibacterial efficiency of AgNPs can be explained by four main pathways: the production of reactive oxygen species (ROS) as a result of redox reactions [88]; adherence of AgNPs to the membranes of bacterial cells [89]; disruption of the membranes [90]; intercalation of AgNPs between DNA bases resulting in blockage of DNA replication and transcription [91]; and accordingly, the disruption of ribosomes, which prevents protein synthesis [92]. In addition, the bacterial cell grievd severe damage as a result of the discharge of internal metabolites triggered by the nanoparticle's passage through the cell membrane, which generated the antibacterial action [93]. The MIC concentration of biogenic AgNPs against *E. coli* strain was found to be 40  $\mu\text{g}/\text{disk}$ , while it was detected to be 20  $\mu\text{g}/\text{disk}$  against *C. albicans* strain. The MIC concentration of biogenic AgNPs was tested for the synergistic activity with tigecycline, linezolid, and clotrimazole antimicrobial agents against the tested strains. The MBC of the biogenic AgNPs was found to be 80  $\mu\text{g}/\text{disk}$  against *E. coli* strain, whereas MFC was detected to be 40  $\mu\text{g}/\text{disk}$  against *C. albicans* strain.

**Table 2.** Screening of antimicrobial efficiency of green synthesized AgNPs.

Microbial Strains	Inhibition Zone Diameter (mm)		
	AgNPs (200 $\mu\text{g}/\text{Disk}$ )	Positive Control	Negative Control
MRSA	28.17 $\pm$ 0.21	20.56 $\pm$ 0.23 (TGC)	0.00 $\pm$ 0.00
<i>A. baumannii</i>	21.04 $\pm$ 0.19	20.63 $\pm$ 0.21 (TGC)	0.00 $\pm$ 0.00
<i>E. coli</i>	36.14 $\pm$ 0.67	22.67 $\pm$ 0.43 (TGC)	0.00 $\pm$ 0.00
<i>C. albicans</i>	18.16 $\pm$ 0.14	21.97 $\pm$ 0.52 (CLO)	0.00 $\pm$ 0.00

TGC: tigecycline, CLO: clotrimazole.

### 3.8. Investigation of the Ultrastructural Changes of Microbial Cells Treated with AgNPs Using SEM Analysis

Figure 11 showed both untreated and AgNP-treated *C. albicans* cells. The treated candidal cells showed distorted characteristics, such as enlarged cells with shriveled cell walls. Furthermore, the SEM investigation showed the deformations of the treated candidal cells with the appearance of cellular remains resulting from the cell wall and cell membrane disruption and, consequently, cell lysis. In addition, SEM examination of AgNPs-treated MRSA cells showed that these cells had an irregular cell shape, with pits and bulges on the cell surface. This might be due to AgNP accumulation over the bacterial cell wall, causing its disruption and the leakage of the cellular constituents and, ultimately, cell death (Figure 12). The control MRSA cells, on the other hand, showed no indications of deformation and were spherical and undamaged. Additionally, the AgNP-treated *E. coli* cells showed signs of damage, including a cracked and wrinkled outer surface and totally warped cell membranes, in contrast to the unaffected control cells, which remained intact. The disruption of cell membranes might be due to AgNP accretion in the bacterial membrane, which causes a shift in membrane potential. As a result, a shift in membrane potential encourages pit development in the membrane and additional cell lysis, ultimately leading to cell death [94].

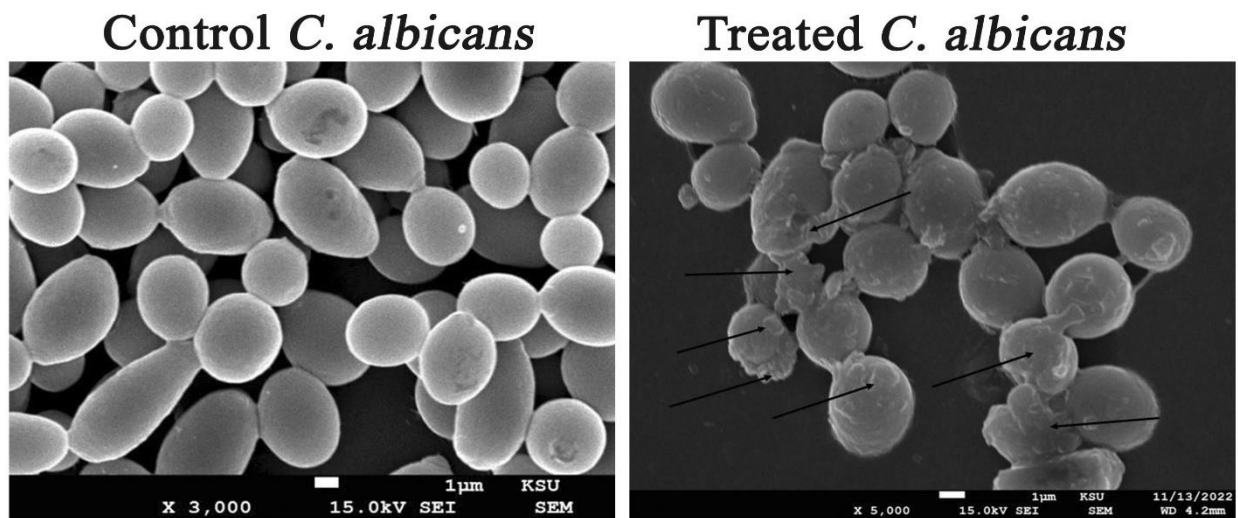


Figure 11. Ultrastructural deformations of *C. albicans* treated with AgNPs.

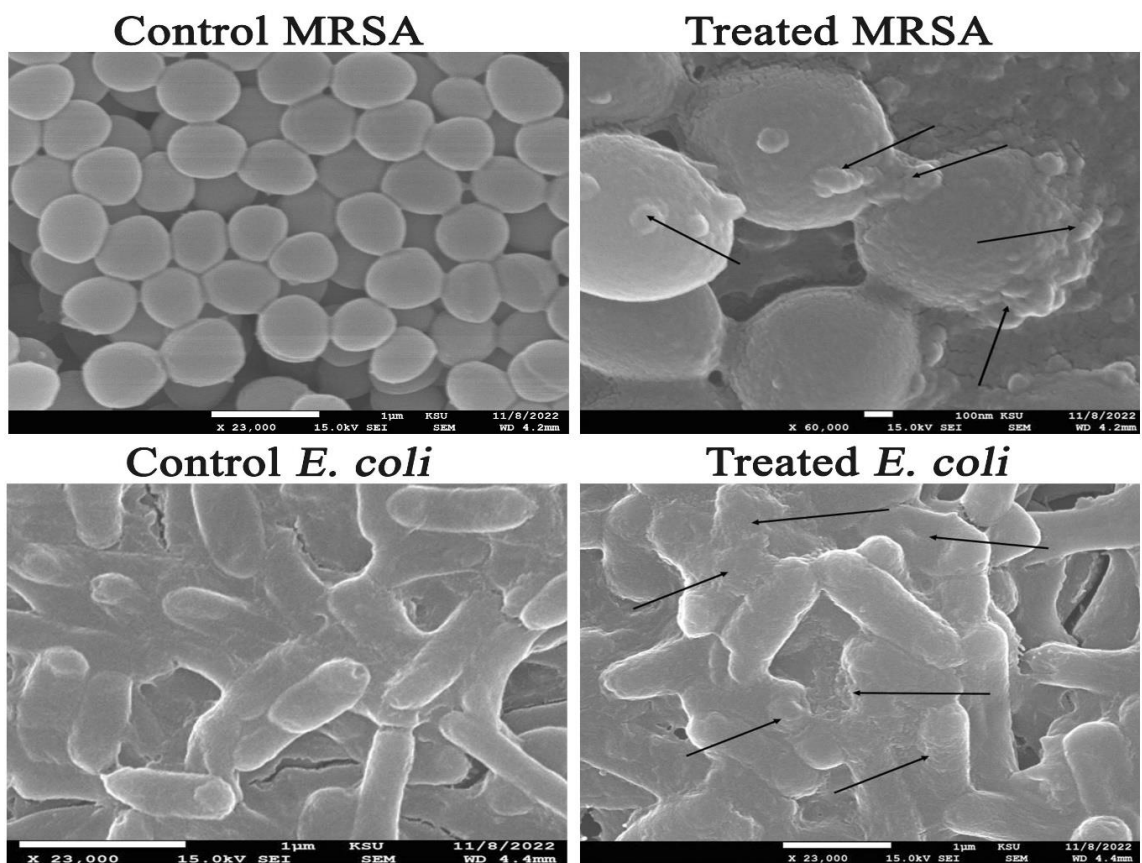


Figure 12. Ultrastructural deformations of MRSA and *E. coli* strains treated with AgNPs.

### 3.9. Synergistic Patterns of AgNPs with Commercial Antimicrobial Agents

The synergistic activity of the biogenic AgNPs with commercial antimicrobial drugs was evaluated. According to the results of the synergetic activity assay, the biofabricated AgNPs (40 µg/disk) demonstrated synergistic efficiency with the antibiotic tigecycline against the strains of *A. baumannii* and *E. coli*, with relative synergism percentages of 8.93 and 15.72%, respectively (Figure 13). In contrast, no effect was detected between AgNPs and tigecycline antibiotic against MRSA strain. The inhibitory zone of the antibiotic tigecycline against MRSA strain was found to be  $20.56 \pm 0.23$  mm, whereas the inhibition zone of the combination of AgNPs and tigecycline was found to be  $19.89 \pm 0.31$  mm. As

a result, the synergistic action was tested with another commercial antibacterial drug, namely, linezolid. According to Table 3, the combined action of linezolid and AgNPs revealed synergistic activity with a percentage of 12.26%. On the other hand, the synergistic antifungal efficacy of AgNPs with clotrimazole antifungal agent was assessed against *C. albicans* strain, and the results showed that the biofabricated AgNPs (20 µg/disk) exposed synergistic potency, which recorded a relative percentage of 8.58%. In addition, the zone of inhibition of tigecycline was found to increase significantly in the synergism test of *E. coli* plates compared to the initial screening test, which recorded relative inhibitory zones of  $35.24 \pm 1.49$  and  $22.67 \pm 0.18$  mm, respectively, demonstrating the potent synergistic activity of AgNPs with tigecycline even at MIC concentration against *E. coli* strain. The synergistic patterns were found to be low, and the synergism was tested between the MIC concentration of silver nanoparticles and different antimicrobial agents. Hence, we tested the synergistic percentages of two-fold MIC concentration of AgNPs with different antimicrobial agents against *E. coli*, *A. baumannii*, MRSA, and *C. albicans* strains. The two-fold MIC concentration of AgNPs revealed relative synergistic percentages of 48.14, 31.60, 29.70, and 39.30% with different antimicrobial agents against *A. baumannii*, *E. coli*, MRSA, and *C. albicans* strains, respectively. Consequently, the findings supported that the relative synergistic activity was increasing with increasing the concentration of the biogenic AgNPs against the tested strains. The highest synergistic action was seen for AgNPs (2-fold MIC) and tigecycline combination against *A. baumannii*, with an IFA of 1.2, whereas the lowest synergism was observed for AgNPs (two-fold MIC) and linezolid combination, with an IFA of 0.7. Nevertheless, weak synergism was identified between AgNPs (MIC) and tigecycline against *A. baumannii* and *E. coli*, with an IFA value of 0.2, while AgNPs (MIC) and linezolid combination showed an IFA value of 0.3 against MRSA strain. The IFA value increased from 0.2 to 0.9 for AgNPs (MIC)-clotrimazole and AgNPs (two-fold MIC)-clotrimazole combinations, respectively. The fractional inhibitory concentration (FIC) index was calculated to detect the synergistic, additive, or antagonistic effect of the biogenic AgNPs (Table 4). The results of FIC revealed the synergistic activity of AgNPs+ tigecycline combination against *A. baumannii* strain, whereas an additive effect was found for both AgNPs+ linezolid and AgNPs+ tigecycline combination against MRSA and *E. coli* strains with FICI value of 0.38, 0.86, and 0.63 respectively. On the other hand, no effect was detected for AgNPs+ tigecycline combination against the MRSA strain with an FICI value of 1.75. Antifungal synergism of AgNPs+ clotrimazole combination against *C. albicans* strain was detected, recording an FICI value of 0.25.

**Table 3.** Synergistic activity of different concentrations of biogenic AgNPs with commercial antibacterial and antifungal agents against the tested microbes.

The Tested Strains	Inhibition Zone Diameter (mm)				
	Antimicrobial Agent	AgNPs (MIC)	AgNPs (MIC) + Antimicrobial Agent	Synergism %	IFA
MRSA	29.18 ± 0.23 (LZD)	18.14 ± 0.18	32.76 ± 0.56	12.26%	0.3
<i>A. baumannii</i>	19.24 ± 0.16 (TGC)	11.23 ± 0.74	20.96 ± 0.42	8.93%	0.2
<i>E. coli</i>	35.24 ± 0.29 (TGC)	19.23 ± 0.37	38.78 ± 0.38	10.04%	0.2
<i>C. albicans</i>	20.98 ± 0.42 (CLO)	8.67 ± 0.67	22.78 ± 0.35	8.58%	0.2
	Antimicrobial Agent	AgNPs (2-fold MIC)	AgNPs (2-fold MIC) + Antimicrobial Agent	Synergism %	IFA
MRSA	29.46 ± 0.11 (LZD)	24.14 ± 0.23	38.21 ± 0.36	29.70%	0.7
<i>A. baumannii</i>	19.67 ± 0.15 (TGC)	16.78 ± 0.46	29.14 ± 0.17	48.14%	1.2
<i>E. coli</i>	35.09 ± 0.29 (TGC)	25.56 ± 0.31	46.18 ± 0.56	31.60%	0.8
<i>C. albicans</i>	20.48 ± 0.54 (CLO)	14.97 ± 0.27	28.53 ± 0.48	39.30%	0.9

LZD: linezolid, TGC: tigecycline, CLO: clotrimazole.

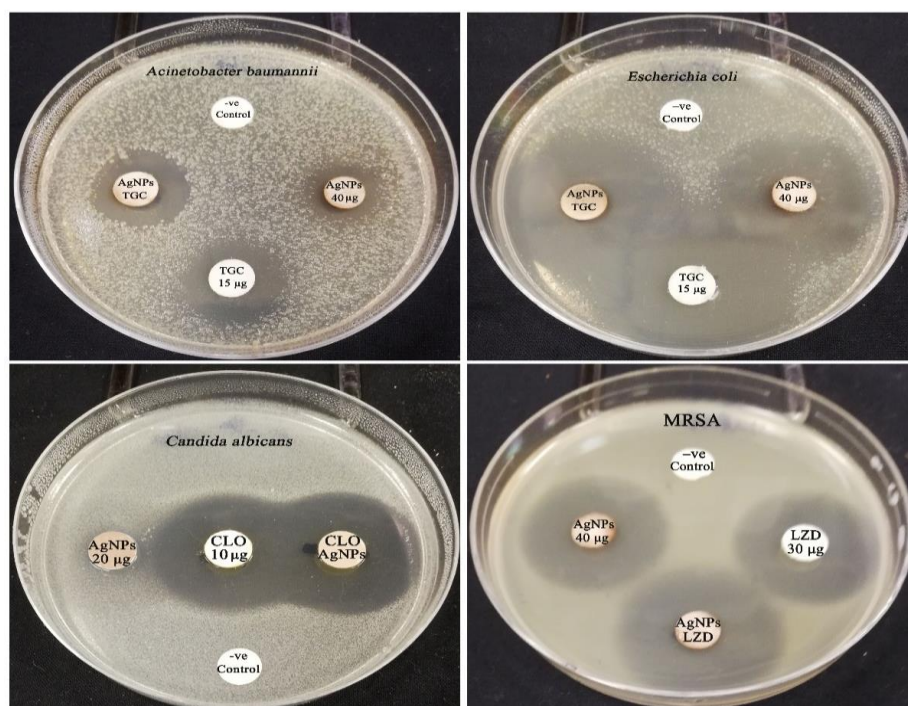


**Figure 13.** Antimicrobial activity of the biogenic AgNPs and commercial antimicrobial agents (LZD: linezolid, TGC: tigecycline, CLO: clotrimazole).

**Table 4.** The fractional inhibitory concentration index (FICI) of the combined AgNPs and antibiotics.

The Tested Strains	Combined AgNPs + Antimicrobial Agent	FICI	Action
MRSA	AgNPs + TGC	1.75	No effect
	AgNPs + LZD	0.86	Additive
<i>A. baumannii</i>	AgNPs + TGC	0.38	Synergistic
<i>E. coli</i>	AgNPs + TGC	0.63	Additive
<i>C. albicans</i>	AgNPs + CLO	0.25	Synergistic

Synergistic effect  $\leq 0.5$ ; additive 0.5 to 1; no effect  $>1$  to 4 and antagonistic  $>4$ . LZD: linezolid, TGC: tigecycline, CLO: clotrimazole.

The synergistic and additive activities of the biogenic AgNPs with tigecycline antibiotic against both gram-negative strains, *A. baumannii* and *E. coli*, were detected, while no effect of this combination was registered against the MRSA strain. We hypothesized that the synergistic effect of biogenic AgNPs in combination with the antibiotic tigecycline could be attributed to the fact that both AgNPs and tigecycline targeted different bacterial cellular components. Tigecycline is a parenterally administered, bacteriostatic glycylycine antibiotic that resembles tetracyclines structurally and has a greater (five-fold) binding affinity [95]. The main antibacterial mode of action of tigecycline is through the inhibition of the protein translation process of bacterial cells as the disruption of peptide chain elongation via reversible binding to a helical region (H34) on the 30S subunit of bacterial ribosomes [96]. Accordingly, tigecycline binding suppressed amino acid residues from being incorporated into peptide chains, which inhibits peptide synthesis and bacterial growth [97]. Based on the preceding, the supposed mechanism of AgNPs–tigecycline involves the action of AgNPs on the disruption of bacterial cell walls and membranes through the action of ROS, which also negatively disrupts bacterial DNA replication, while the tigecycline antibiotic suppresses bacterial protein translation and stops bacterial growth, leading to a synergistic shut down of biological activities of bacterial cells and induction of microbial cell death. The additive effect of linezolid antibiotic with biogenic AgNPs against MRSA strain was

detected, whereas tigecycline antibiotic did not show any synergism with AgNPs against MRSA. Linezolid is the first antibacterial agent in the oxazolidinone class, which is used to treat nosocomial pneumonia, as well as mild and serious skin and soft tissue infections initiated by certain gram-positive bacteria [98]. In this context, linezolid inhibited bacterial protein synthesis by binding to rRNA on both the 50S and 30S ribosomal subunits, whereas AgNPs disrupted membrane permeability via ROS action and interrupted bacterial DNA replication, resulting in additive antibacterial activity when combined with linezolid. On the other hand, the biogenic AgNPs showed synergistic activity with the antifungal drug clotrimazole, disrupting the synthesis of ergosterol, the primary component of fungal cells' membranes, depleting it, and replacing it with the aberrant sterol species 14-methylsterol, which then impairs membrane fluidity and permeability [99]. Additionally, the biogenic AgNPs exhibited an antifungal mode of action through interactions with DNA and protein, which disrupted these molecules and caused cell death, which then worked in a synergistic way with clotrimazole against *C. albicans* strain [100].

#### 4. Conclusions

The biogenic AgNPs exhibited antibacterial and anticandidal activities against the tested strains. Ultrastructural investigation affirmed the deformation and distortion of bacterial and candidal cells treated with the biogenic AgNPs. The high efficiency of the biogenic AgNPs might be attributed to the small particle size of AgNPs, which enables them to penetrate the cell, and also to the action of capping biomolecules adsorbed over the surface of AgNPs. The biogenic AgNPs revealed the highest synergism with tigecycline against *A. baumannii*, which indicated the possible use of this combination for control of the multidrug-resistant pathogens colonizing the surfaces in ICUs and hospitals. In addition, tigecycline and linezolid exposed additive antibacterial efficacy with the bioinspired AgNPs against *E. coli* and MRSA strains, respectively. The biosynthesized AgNPs also exposed a synergistic activity with clotrimazole against *C. albicans*, indicating the possible usage of this combination to control the candidal colonization of medical equipment in ICUs and healthcare settings.

**Author Contributions:** Conceptualization, M.T.Y. and A.A.A.-A.; methodology, M.T.Y.; software, M.T.Y.; validation, M.T.Y. and F.O.A.-O.; formal analysis, A.A.A.-A. and F.O.A.-O.; investigation, M.T.Y.; resources, A.A.A.-A.; data curation, M.T.Y. and K.M.; writing—original draft preparation, M.T.Y.; writing—review and editing, M.T.Y., A.A.A.-A. and F.O.A.-O.; visualization, F.O.A.-O.; supervision, A.A.A.-A. and F.O.A.-O.; project administration, A.A.A.-A. and F.O.A.-O.; funding acquisition, F.O.A.-O. All authors have read and agreed to the published version of the manuscript.

**Funding:** The study was funded by the Deputyship for Research & Innovation, Ministry of Education in Saudi Arabia, through project no. (IFKSURG-2-1554).

**Data Availability Statement:** All required data are present in this file.

**Acknowledgments:** The authors extend their appreciation to the Deputyship for Research & Innovation, Ministry of Education in Saudi Arabia, for funding this research work through project no. (IFKSURG-2-1554).

**Conflicts of Interest:** The authors declare no conflict of interest.

#### References

1. Schechner, V.; Wulffhart, L.; Temkin, E.; Feldman, S.F.; Nutman, A.; Shitrit, P.; Schwaber, M.J.; Carmeli, Y. One-Year Mortality and Years of Potential Life Lost Following Bloodstream Infection among Adults: A Nation-Wide Population Based Study. *Lancet Reg. Health-Eur.* **2022**, *23*, 100511. [[CrossRef](#)] [[PubMed](#)]
2. Sheikh Omar, N.M.; Erismis, B.; Muse Osman, M.; Garba, B.; Hassan, M.A.; Akuku, I.G. Retrospective Evaluation of Nosocomial Bacterial Infections and Their Antimicrobial Resistance Patterns Among Hospitalized Patients in Mogadishu, Somalia. *Infect. Drug Resist.* **2023**, *16*, 705–720. [[CrossRef](#)] [[PubMed](#)]
3. Tiwari, P.; Deshwal, P.R. Emerging Infections and Their Management. In *Drug Repurposing for Emerging Infectious Diseases and Cancer*; Springer: Berlin/Heidelberg, Germany, 2023; pp. 593–614.

4. Nimer, N.A. Nosocomial Infection and Antibiotic-Resistant Threat in the Middle East. *Infect. Drug Resist.* **2022**, *15*, 631–639. [[CrossRef](#)] [[PubMed](#)]
5. Han, Y.; Zhang, J.; Zhang, H.-Z.; Zhang, X.-Y.; Wang, Y.-M. Multidrug-Resistant Organisms in Intensive Care Units and Logistic Analysis of Risk Factors. *World J. Clin. Cases* **2022**, *10*, 1795. [[CrossRef](#)]
6. Ananda, T.; Modi, A.; Chakraborty, I.; Managuli, V.; Mukhopadhyay, C.; Mazumder, N. Nosocomial Infections and Role of Nanotechnology. *Bioengineering* **2022**, *9*, 51. [[CrossRef](#)]
7. Bhatta, D.R.; Koirala, S.; Baral, A.; Amatya, N.M.; Parajuli, S.; Shrestha, R.; Hamal, D.; Nayak, N.; Gokhale, S. Methicillin-Resistant *Staphylococcus aureus* Contamination of Frequently Touched Objects in Intensive Care Units: Potential Threat of Nosocomial Infections. *Can. J. Infect. Dis. Med. Microbiol.* **2022**, *2022*, e1023241. [[CrossRef](#)]
8. Ludden, C.; Coll, F.; Gouliouris, T.; Restif, O.; Blane, B.; Blackwell, G.A.; Kumar, N.; Naydenova, P.; Crawley, C.; Brown, N.M.; et al. Defining Nosocomial Transmission of *Escherichia Coli* and Antimicrobial Resistance Genes: A Genomic Surveillance Study. *Lancet Microbe* **2021**, *2*, e472–e480. [[CrossRef](#)]
9. Nguyen, M.; Joshi, S.G. Carbapenem Resistance in *Acinetobacter baumannii*, and Their Importance in Hospital-Acquired Infections: A Scientific Review. *J. Appl. Microbiol.* **2021**, *131*, 2715–2738. [[CrossRef](#)]
10. Muzaaheed; Alshehri, B.A.; Rabaan, A.A.; El-Masry, O.S.; Acharya, S.; Alzahrani, F.M.; Al Mutair, A.; Alhumaid, S.; Al-Tawfiq, J.A.; Muhammad, J.; et al. A 20-Year Retrospective Clinical Analysis of Candida Infections in Tertiary Centre: Single-Center Experience. *J. Infect. Public Health* **2022**, *15*, 69–74. [[CrossRef](#)]
11. Parmanik, A.; Das, S.; Kar, B.; Bose, A.; Dwivedi, G.R.; Pandey, M.M. Current Treatment Strategies Against Multidrug-Resistant Bacteria: A Review. *Curr. Microbiol.* **2022**, *79*, 388. [[CrossRef](#)]
12. Kothari, A.; Kumar, P.; Gaurav, A.; Kaushal, K.; Pandey, A.; Yadav, S.R.M.; Jain, N.; Omar, B.J. Association of Antibiotics and Heavy Metal Arsenic to Horizontal Gene Transfer from Multidrug-Resistant Clinical Strains to Antibiotic-Sensitive Environmental Strains. *J. Hazard. Mater.* **2022**, *443*, 130260. [[CrossRef](#)]
13. Wang, D.; Ning, Q.; Deng, Z.; Zhang, M.; You, J. Role of Environmental Stresses in Elevating Resistance Mutations in Bacteria: Phenomena and Mechanisms. *Environ. Pollut.* **2022**, *307*, 119603. [[CrossRef](#)]
14. Murugaiyan, J.; Kumar, P.A.; Rao, G.S.; Iskandar, K.; Hawser, S.; Hays, J.P.; Mohsen, Y.; Adukkadukkam, S.; Awuah, W.A.; Jose, R.A.M.; et al. Progress in Alternative Strategies to Combat Antimicrobial Resistance: Focus on Antibiotics. *Antibiotics* **2022**, *11*, 200. [[CrossRef](#)]
15. Sharma, M.; Chauhan, P.; Sharma, R.; Kumar, D. Application of Nanotechnology in Clinical Research: Present and Future Prospects. *Nanomater. Clin. Ther. Synth. Appl.* **2022**, *3*, 75–113. [[CrossRef](#)]
16. Singh, R.; Sharma, A.; Saji, J.; Umaphathi, A.; Kumar, S.; Daima, H.K. Smart Nanomaterials for Cancer Diagnosis and Treatment. *Nano Converg.* **2022**, *9*, 21. [[CrossRef](#)]
17. Rezaee, T.; Fazel-Zarandi, R.; Karimi, A.; Ensafi, A.A. Metal-Organic Frameworks for Pharmaceutical and Biomedical Applications. *J. Pharm. Biomed. Anal.* **2022**, *221*, 115026. [[CrossRef](#)]
18. Rajamanickam, K. Application of Quantum Dots in Bio-Sensing, Bio-Imaging, Drug Delivery, Anti-Bacterial Activity, Photo-Thermal, Photo-Dynamic Therapy, and Optoelectronic Devices. In *Quantum Dots-Recent Advances, New Perspectives and Contemporary Applications*; IntechOpen: London, UK, 2022.
19. Vassallo, A.; Silletti, M.F.; Faraone, I.; Milella, L. Nanoparticulate Antibiotic Systems as Antibacterial Agents and Antibiotic Delivery Platforms to Fight Infections. *J. Nanomater.* **2020**, *2020*, 1–31. [[CrossRef](#)]
20. Binsalah, M.; Devanesan, S.; AlSalhi, M.S.; Nooh, A.; Alghamdi, O.; Nooh, N. Biomimetic Synthesis of Silver Nanoparticles Using Ethyl Acetate Extract of *Urtica Diocia* Leaves; Characterizations and Emerging Antimicrobial Activity. *Microorganisms* **2022**, *10*, 789. [[CrossRef](#)]
21. Saeki, E.K.; Martins, H.M.; de Camargo, L.C.; Anversa, L.; Tavares, E.R.; Yamada-Ogatta, S.F.; Lioni, L.M.Y.; Kobayashi, R.K.T.; Nakazato, G. Effect of Biogenic Silver Nanoparticles on the Quorum-Sensing System of *Pseudomonas aeruginosa* PAO1 and PA14. *Microorganisms* **2022**, *10*, 1755. [[CrossRef](#)]
22. Simon, S.; Sibuyi, N.R.S.; Fadaka, A.O.; Meyer, S.; Josephs, J.; Onani, M.O.; Meyer, M.; Madiehe, A.M. Biomedical Applications of Plant Extract-Synthesized Silver Nanoparticles. *Biomedicines* **2022**, *10*, 2792. [[CrossRef](#)]
23. Khane, Y.; Benouis, K.; Albukhaty, S.; Sulaiman, G.M.; Abomughaid, M.M.; Al Ali, A.; Aouf, D.; Fenniche, F.; Khane, S.; Chaibi, W. Green Synthesis of Silver Nanoparticles Using Aqueous Citrus Limon Zest Extract: Characterization and Evaluation of Their Antioxidant and Antimicrobial Properties. *Nanomaterials* **2022**, *12*, 2013. [[CrossRef](#)] [[PubMed](#)]
24. Rasool, S.; Tayyeb, A.; Raza, M.A.; Ashfaq, H.; Perveen, S.; Kanwal, Z.; Riaz, S.; Naseem, S.; Abbas, N.; Ahmad, N. Citrullus Colocynthis-Mediated Green Synthesis of Silver Nanoparticles and Their Antiproliferative Action against Breast Cancer Cells and Bactericidal Roles against Human Pathogens. *Nanomaterials* **2022**, *12*, 3781. [[CrossRef](#)] [[PubMed](#)]
25. Yassin, M.T.; Mostafa, A.A.-F.; Al-Askar, A.A.; Al-Otibi, F.O. Facile Green Synthesis of Silver Nanoparticles Using Aqueous Leaf Extract of *Origanum Majorana* with Potential Bioactivity against Multidrug Resistant Bacterial Strains. *Crystals* **2022**, *12*, 603. [[CrossRef](#)]
26. Almaary, K.S.; Yassin, M.T.; Elgorban, A.M.; Al-Otibi, F.O.; Al-Askar, A.A.; Maniah, K. Synergistic Antibacterial Proficiency of Green Bioformulated Zinc Oxide Nanoparticles with Potential Fosfomycin Synergism against Nosocomial Bacterial Pathogens. *Microorganisms* **2023**, *11*, 645. [[CrossRef](#)]

27. Yassin, M.T.; Mostafa, A.A.-F.; Al-Askar, A.A.; Al-Otibi, F.O. Synergistic Antifungal Efficiency of Biogenic Silver Nanoparticles with Itraconazole against Multidrug-Resistant Candidal Strains. *Crystals* **2022**, *12*, 816. [[CrossRef](#)]
28. Yassin, M.T.; Mostafa, A.A.-F.; Al-Askar, A.A.; Al-Otibi, F.O. Synergistic Antibacterial Activity of Green Synthesized Silver Nanomaterials with Colistin Antibiotic against Multidrug-Resistant Bacterial Pathogens. *Crystals* **2022**, *12*, 1057. [[CrossRef](#)]
29. Aljeldah, M.M.; Yassin, M.T.; Mostafa, A.A.-F.; Aboul-Soud, M.A. Synergistic Antibacterial Potential of Greenly Synthesized Silver Nanoparticles with Fosfomycin Against Some Nosocomial Bacterial Pathogens. *Infect. Drug Resist.* **2023**, *16*, 125–142. [[CrossRef](#)]
30. Barabadi, H.; Mojab, F.; Vahidi, H.; Marashi, B.; Talank, N.; Hosseini, O.; Saravanan, M. Green Synthesis, Characterization, Antibacterial and Biofilm Inhibitory Activity of Silver Nanoparticles Compared to Commercial Silver Nanoparticles. *Inorg. Chem. Commun.* **2021**, *129*, 108647. [[CrossRef](#)]
31. Narayanan, M.; Divya, S.; Natarajan, D.; Senthil-Nathan, S.; Kandasamy, S.; Chinnathambi, A.; Alahmadi, T.A.; Pugazhendhi, A. Green Synthesis of Silver Nanoparticles from Aqueous Extract of *Ctenolepis Garcini* L. and Assess Their Possible Biological Applications. *Process Biochem.* **2021**, *107*, 91–99. [[CrossRef](#)]
32. Mehwish, H.M.; Rajoka, M.S.R.; Xiong, Y.; Cai, H.; Aadil, R.M.; Mahmood, Q.; He, Z.; Zhu, Q. Green Synthesis of a Silver Nanoparticle Using *Moringa oleifera* Seed and Its Applications for Antimicrobial and Sun-Light Mediated Photocatalytic Water Detoxification. *J. Environ. Chem. Eng.* **2021**, *9*, 105290. [[CrossRef](#)]
33. Aabed, K.; Mohammed, A.E. Synergistic and Antagonistic Effects of Biogenic Silver Nanoparticles in Combination with Antibiotics Against Some Pathogenic Microbes. *Front. Bioeng. Biotechnol.* **2021**, *9*, 652362. [[CrossRef](#)]
34. Huang, W.; Wang, J.; Wang, Z.; Yu, H. Synergistic Antimicrobial Activity of Silver Nanoparticles Combined with Streptomycin Sulfate against Gram-Negative and Gram-Positive Bacteria. *Mol. Cryst. Liq. Cryst.* **2021**, *714*, 80–88. [[CrossRef](#)]
35. Lopez-Carrizales, M.; Velasco, K.I.; Castillo, C.; Flores, A.; Magaña, M.; Martinez-Castanon, G.A.; Martinez-Gutierrez, F. In Vitro Synergism of Silver Nanoparticles with Antibiotics as an Alternative Treatment in Multiresistant Uropathogens. *Antibiotics* **2018**, *7*, 50. [[CrossRef](#)]
36. Allend, S.O.; Garcia, M.O.; da Cunha, K.F.; de Albernaz, D.T.F.; da Silva, M.E.; Ishikame, R.Y.; Panagio, L.A.; Nakazaro, G.; Reis, G.F.; Pereira, D.B.; et al. Biogenic Silver Nanoparticle (Bio-AgNP) Has an Antibacterial Effect against Carbapenem-resistant *Acinetobacter baumannii* with Synergism and Additivity When Combined with Polymyxin B. *J. Appl. Microbiol.* **2022**, *132*, 1036–1047. [[CrossRef](#)]
37. Yassin, M.T.; Elgorban, A.M.; Al-Askar, A.A.; Sholkamy, E.N.; Ameen, F.; Maniah, K. Synergistic Anticandidal Activities of Greenly Synthesized ZnO Nanomaterials with Commercial Antifungal Agents against Candidal Infections. *Micromachines* **2023**, *14*, 209. [[CrossRef](#)]
38. Widatalla, H.A.; Yassin, L.F.; Alrasheid, A.A.; Ahmed, S.A.R.; Widdatallah, M.O.; Eltilib, S.H.; Mohamed, A.A. Green Synthesis of Silver Nanoparticles Using Green Tea Leaf Extract, Characterization and Evaluation of Antimicrobial Activity. *Nanoscale Adv.* **2022**, *4*, 911–915. [[CrossRef](#)]
39. Nakhjavani, M.; Nikkhah, V.; Sarafraz, M.M.; Shoja, S.; Sarafraz, M. Green Synthesis of Silver Nanoparticles Using Green Tea Leaves: Experimental Study on the Morphological, Rheological and Antibacterial Behaviour. *Heat Mass Transf.* **2017**, *53*, 3201–3209. [[CrossRef](#)]
40. Yassin, M.T.; Mostafa, A.A.; Al-Askar, A.A. Anticandidal and Anti-Carcinogenic Activities of *Mentha Longifolia* (Wild Mint) Extracts in Vitro. *J. King Saud Univ. Sci.* **2020**, *32*, 2046–2052. [[CrossRef](#)]
41. Yassin, M.T.; Mostafa, A.A.-F.; Al-Askar, A.A. In Vitro Anticandidal Potency of *Syzygium aromaticum* (Clove) Extracts against Vaginal Candidiasis. *BMC Complement. Med. Ther.* **2020**, *20*, 25. [[CrossRef](#)]
42. Yassin, M.; Mostafa, A.A.; Al-Askar, A. Anticandidal Efficiency of Cinnamomum Zeylanicum Extracts against Vulvovaginal Candidiasis. *Curr. Sci.* **2020**, *118*, 796–801. [[CrossRef](#)]
43. Yassin, M.T.; Mostafa, A.A.-F.; Al-Askar, A.A.; Al-Otibi, F.O. Facile Green Synthesis of Zinc Oxide Nanoparticles with Potential Synergistic Activity with Common Antifungal Agents against Multidrug-Resistant Candidal Strains. *Crystals* **2022**, *12*, 774. [[CrossRef](#)]
44. Yassin, M.T.; Al-Askar, A.A.; Maniah, K.; Al-Otibi, F.O. Green Synthesis of Zinc Oxide Nanocrystals Utilizing *Origanum Majorana* Leaf Extract and Their Synergistic Patterns with Colistin against Multidrug-Resistant Bacterial Strains. *Crystals* **2022**, *12*, 1513. [[CrossRef](#)]
45. Njume, C.; Afolayan, A.J.; Green, E.; Ndip, R.N. Volatile Compounds in the Stem Bark of *Sclerocarya birrea* (Anacardiaceae) Possess Antimicrobial Activity against Drug-Resistant Strains of *Helicobacter Pylori*. *Int. J. Antimicrob. Agents* **2011**, *38*, 319–324. [[CrossRef](#)] [[PubMed](#)]
46. Yassin, M.T.; Mostafa, A.A.-F.; Al-Askar, A.A. In Vitro Evaluation of Biological Activities and Phytochemical Analysis of Different Solvent Extracts of *Punica granatum* L. (Pomegranate) Peels. *Plants* **2021**, *10*, 2742. [[CrossRef](#)] [[PubMed](#)]
47. Singh, R.; Wagh, P.; Wadhvani, S.; Gaidhani, S.; Kumbhar, A.; Bellare, J.; Chopade, B.A. Synthesis, Optimization, and Characterization of Silver Nanoparticles from *Acinetobacter Calcoaceticus* and Their Enhanced Antibacterial Activity When Combined with Antibiotics. *Int. J. Nanomed.* **2013**, *8*, 4277–4290. [[CrossRef](#)]
48. Ma, L.; Qiu, S.; Chen, K.; Tang, J.; Liu, J.; Su, W.; Liu, X.; Zeng, X. Synergistic Antibacterial Effect from Silver Nanoparticles and Anticancer Activity Against Human Lung Cancer Cells. *J. Biomed. Nanotechnol.* **2022**, *18*, 2204–2215. [[CrossRef](#)]
49. Haji, S.H.; Ali, F.A.; Aka, S.T.H. Synergistic Antibacterial Activity of Silver Nanoparticles Biosynthesized by Carbapenem-Resistant Gram-Negative Bacilli. *Sci. Rep.* **2022**, *12*, 15254. [[CrossRef](#)]

50. Ben Khalifa, R.; Cacciatore, I.; Dimmito, M.P.; Ciulla, M.; Grande, R.; Puca, V.; Robuffo, I.; De Laurenzi, V.; Chekir-Ghedira, L.; Di Stefano, A.; et al. Multiple Lipid Nanoparticles as Antimicrobial Drug Delivery Systems. *J. Drug Deliv. Sci. Technol.* **2022**, *67*, 102887. [[CrossRef](#)]
51. Xu, Q.; Li, W.; Weng, X.; Owens, G.; Chen, Z. Mechanism and Impact of Synthesis Conditions on the One-Step Green Synthesis of Hybrid RGO@Fe/Pd Nanoparticles. *Sci. Total Environ.* **2020**, *710*, 136308. [[CrossRef](#)]
52. Alahmad, A.; Al-Zereini, W.A.; Hijazin, T.J.; Al-Madanat, O.Y.; Alghoraibi, I.; Al-Qaralleh, O.; Al-Qaraleh, S.; Feldhoff, A.; Walter, J.-G.; Scheper, T. Green Synthesis of Silver Nanoparticles Using *Hypericum perforatum* L. Aqueous Extract with the Evaluation of Its Antibacterial Activity against Clinical and Food Pathogens. *Pharmaceutics* **2022**, *14*, 1104. [[CrossRef](#)]
53. Hussain, M.; Nafady, A.; Avci, A.; Pehlivan, E.; Nisar, J.; Sherazi, S.T.H.; Balouch, A.; Shah, M.R.; Almaghrabi, O.A.; Ul-Haq, M.A. Biogenic Silver Nanoparticles for Trace Colorimetric Sensing of Enzyme Disrupter Fungicide Vinclozolin. *Nanomaterials* **2019**, *9*, 1604. [[CrossRef](#)]
54. Ali, M.; Kim, B.; Belfield, K.D.; Norman, D.; Brennan, M.; Ali, G.S. Green Synthesis and Characterization of Silver Nanoparticles Using Artemisia Absinthium Aqueous Extract—A Comprehensive Study. *Mater. Sci. Eng. C* **2016**, *58*, 359–365. [[CrossRef](#)]
55. Rolim, W.R.; Pelegrino, M.T.; de Araújo Lima, B.; Ferraz, L.S.; Costa, F.N.; Bernardes, J.S.; Rodrigues, T.; Brocchi, M.; Seabra, A.B. Green Tea Extract Mediated Biogenic Synthesis of Silver Nanoparticles: Characterization, Cytotoxicity Evaluation and Antibacterial Activity. *Appl. Surf. Sci.* **2019**, *463*, 66–74. [[CrossRef](#)]
56. Saini, P.; Saha, S.K.; Roy, P.; Chowdhury, P.; Sinha Babu, S.P. Evidence of Reactive Oxygen Species (ROS) Mediated Apoptosis in *Setaria Cervi* Induced by Green Silver Nanoparticles from *Acacia Auriculiformis* at a Very Low Dose. *Exp. Parasitol.* **2016**, *160*, 39–48. [[CrossRef](#)]
57. Ghiuță, I.; Cristea, D.; Croitoru, C.; Kost, J.; Wenkert, R.; Vyrides, I.; Anayiotos, A.; Munteanu, D. Characterization and Antimicrobial Activity of Silver Nanoparticles, Biosynthesized Using *Bacillus* Species. *Appl. Surf. Sci.* **2018**, *438*, 66–73. [[CrossRef](#)]
58. Riaz, M.; Sharafat, U.; Zahid, N.; Ismail, M.; Park, J.; Ahmad, B.; Rashid, N.; Fahim, M.; Imran, M.; Tabassum, A. Synthesis of Biogenic Silver Nanocatalyst and Their Antibacterial and Organic Pollutants Reduction Ability. *ACS Omega* **2022**, *7*, 14723–14734. [[CrossRef](#)]
59. Khalifa, K.S.; Hamouda, R.; Hamza, D. In Vitro Antitumor Activity of Silver Nanoparticles Biosynthesized by Marine Algae. *Dig. J. Nanomater. Biostruct.* **2016**, *11*, 213–221.
60. Kumar, D.A.; Palanichamy, V.; Roopan, S.M. Green Synthesis of Silver Nanoparticles Using *Alternanthera Dentata* Leaf Extract at Room Temperature and Their Antimicrobial Activity. *Spectrochim. Acta Part A Mol. Biomol. Spectrosc.* **2014**, *127*, 168–171. [[CrossRef](#)]
61. Ahmad, N.; Fozia, U.; Jabeen, M.; Haq, Z.U.; Ahmad, I.; Wahab, A.; Islam, Z.U.; Ullah, R.; Bari, A.; Abdel-Daim, M.M.; et al. Green Fabrication of Silver Nanoparticles Using *Euphorbia Serpens* Kunth Aqueous Extract, Their Characterization, and Investigation of Its In Vitro Antioxidative, Antimicrobial, Insecticidal, and Cytotoxic Activities. *BioMed Res. Int.* **2022**, *2022*, e5562849. [[CrossRef](#)]
62. Khatami, M.; Nejad, M.S.; Salari, S.; Almani, P.G.N. Plant-Mediated Green Synthesis of Silver Nanoparticles Using *Trifolium Resupinatum* Seed Exudate and Their Antifungal Efficacy on *Neofusicoccum Parvum* and *Rhizoctonia Solani*. *IET Nanobiotechnol.* **2016**, *10*, 237–243. [[CrossRef](#)]
63. Ahmed, Q.; Gupta, N.; Kumar, A.; Nimesh, S. Antibacterial Efficacy of Silver Nanoparticles Synthesized Employing *Terminalia Arjuna* Bark Extract. *Artif. Cells Nanomed. Biotechnol.* **2017**, *45*, 1192–1200. [[CrossRef](#)] [[PubMed](#)]
64. Bharathi, E.; Sivakumari, G.; Kamalakkannan, J.; Karthikeyan, B.; Senthilvelan, S. Synergetic Execute Pressure, Temperature on Mixed Ac/Ag@CuO and Its Multi Properties of Solar Light Elucidation and Antibacterial Activity by Hydrothermal Technique. *Mater. Sci. Energy Technol.* **2020**, *3*, 407–419. [[CrossRef](#)]
65. Kumar, A.G.; Sankarganesh, P.; Parthasarathy, V.; Bhuvaneshwari, J.; Anbarasan, R. In-Vitro and in-Vivo Biological Potential of the Prepared *Feroniella Lucida* Mediated Silver Nanoparticles. *J. Sol-Gel Sci. Technol.* **2022**, *101*, 411–419. [[CrossRef](#)]
66. Al Aboody, M.S. Silver/Silver Chloride (Ag/AgCl) Nanoparticles Synthesized from *Azadirachta Indica* Lalex and Its Antibiofilm Activity against Fluconazole Resistant *Candida Tropicalis*. *Artif. Cells Nanomed. Biotechnol.* **2019**, *47*, 2107–2113. [[CrossRef](#)]
67. Singh, H.; Du, J.; Singh, P.; Yi, T.H. Ecofriendly Synthesis of Silver and Gold Nanoparticles by *Euphrasia officinalis* Leaf Extract and Its Biomedical Applications. *Artif. Cells Nanomed. Biotechnol.* **2018**, *46*, 1163–1170. [[CrossRef](#)]
68. Rahman, A.U.; Khan, A.U.; Yuan, Q.; Wei, Y.; Ahmad, A.; Ullah, S.; Khan, Z.U.H.; Shams, S.; Tariq, M.; Ahmad, W. Tuber Extract of *Arisaema flavum* Eco-Benignly and Effectively Synthesize Silver Nanoparticles: Photocatalytic and Antibacterial Response against Multidrug Resistant Engineered *E. Coli* QH4. *J. Photochem. Photobiol. B* **2019**, *193*, 31–38. [[CrossRef](#)]
69. Kumar, V.; Singh, S.; Srivastava, B.; Bhadouria, R.; Singh, R. Green Synthesis of Silver Nanoparticles Using Leaf Extract of *Holoptelea integrifolia* and Preliminary Investigation of Its Antioxidant, Anti-Inflammatory, Antidiabetic and Antibacterial Activities. *J. Environ. Chem. Eng.* **2019**, *7*, 103094. [[CrossRef](#)]
70. Panwar, R.S.; Pervaiz, N.; Dhillon, G.; Kumar, S.; Sharma, N.; Aggarwal, N.; Tripathi, S.; Kumar, R.; Vashisht, A.; Kumar, N. *Mangifera indica* Leaf Extract Assisted Biogenic Silver Nanoparticles Potentiates Photocatalytic Activity and Cytotoxicity. *J. Mater. Sci. Mater. Electron.* **2022**, *33*, 16538–16549. [[CrossRef](#)]
71. Serrano-Lotina, A.; Portela, R.; Baeza, P.; Alcolea-Rodriguez, V.; Villarroel, M.; Ávila, P. Zeta Potential as a Tool for Functional Materials Development. *Catal. Today* **2022**, *31*. [[CrossRef](#)]

72. Chen, P.; Chai, M.; Mai, Z.; Liao, M.; Xie, X.; Lu, Z.; Zhang, W.; Zhao, H.; Dong, X.; Fu, X.; et al. Electrospinning Polyacrylonitrile (PAN) Based Nanofibrous Membranes Synergic with Plant Antibacterial Agent and Silver Nanoparticles (AgNPs) for Potential Wound Dressing. *Mater. Today Commun.* **2022**, *31*, 103336. [[CrossRef](#)]
73. Niloy, M.S.; Hossain, M.M.; Takikawa, M.; Shakil, M.S.; Polash, S.A.; Mahmud, K.M.; Uddin, M.F.; Alam, M.; Shubhra, R.D.; Shawan, M.M.A.K.; et al. Synthesis of Biogenic Silver Nanoparticles Using *Caesalpinia digyna* and Investigation of Their Antimicrobial Activity and In Vivo Biocompatibility. *ACS Appl. Bio Mater.* **2020**, *3*, 7722–7733. [[CrossRef](#)]
74. Jardón-Romero, E.A.; Lara-Carrillo, E.; González-Pedroza, M.G.; Sánchez-Mendieta, V.; Salmerón-Valdés, E.N.; Toral-Rizo, V.H.; Olea-Mejía, O.F.; López-González, S.; Morales-Luckie, R.A. Antimicrobial Activity of Biogenic Silver Nanoparticles from *Syzygium aromaticum* against the Five Most Common Microorganisms in the Oral Cavity. *Antibiotics* **2022**, *11*, 834. [[CrossRef](#)]
75. Gul, A.R.; Shaheen, F.; Rafique, R.; Bal, J.; Waseem, S.; Park, T.J. Grass-Mediated Biogenic Synthesis of Silver Nanoparticles and Their Drug Delivery Evaluation: A Biocompatible Anti-Cancer Therapy. *Chem. Eng. J.* **2021**, *407*, 127202. [[CrossRef](#)]
76. Kim, K.-M.; Song, J.H.; Kim, M.-K.; Chung, S.-T.; Jeong, J.; Yang, J.-Y.; Choi, A.-J.; Choi, H.-J.; Oh, J.-M. Physicochemical Analysis Methods for Nanomaterials Considering Their Toxicological Evaluations. *Mol. Cell. Toxicol.* **2014**, *10*, 347–360. [[CrossRef](#)]
77. Souza, T.G.F.; Ciminelli, V.S.T.; Mohallem, N.D.S. A Comparison of TEM and DLS Methods to Characterize Size Distribution of Ceramic Nanoparticles. *J. Phys. Conf. Ser.* **2016**, *733*, 012039. [[CrossRef](#)]
78. Abdullah, F.H.; Abu Bakar, N.H.H.; Abu Bakar, M. Comparative Study of Chemically Synthesized and Low Temperature Bio-Inspired Musa Acuminata Peel Extract Mediated Zinc Oxide Nanoparticles for Enhanced Visible-Photocatalytic Degradation of Organic Contaminants in Wastewater Treatment. *J. Hazard. Mater.* **2021**, *406*, 124779. [[CrossRef](#)]
79. Zhao, J.; Pinchuk, A.O.; McMahan, J.M.; Li, S.; Ausman, L.K.; Atkinson, A.L.; Schatz, G.C. Methods for Describing the Electromagnetic Properties of Silver and Gold Nanoparticles. *Acc. Chem. Res.* **2008**, *41*, 1710–1720. [[CrossRef](#)]
80. Majoumouo, M.S.; Sharma, J.R.; Sibuyi, N.R.S.; Tincho, M.B.; Boyom, F.F.; Meyer, M. Synthesis of Biogenic Gold Nanoparticles from Terminalia Mantaly Extracts and the Evaluation of Their In Vitro Cytotoxic Effects in Cancer Cells. *Molecules* **2020**, *25*, 4469. [[CrossRef](#)]
81. Rozhin, A.; Batasheva, S.; Kruchkova, M.; Cherednichenko, Y.; Rozhina, E.; Fakhrullin, R. Biogenic Silver Nanoparticles: Synthesis and Application as Antibacterial and Antifungal Agents. *Micromachines* **2021**, *12*, 1480. [[CrossRef](#)]
82. Ali, S.G.; Jalal, M.; Ahmad, H.; Sharma, D.; Ahmad, A.; Umar, K.; Khan, H.M. Green Synthesis of Silver Nanoparticles from *Camellia Sinensis* and Its Antimicrobial and Antibiofilm Effect against Clinical Isolates. *Materials* **2022**, *15*, 6978. [[CrossRef](#)]
83. Leong, C.Y.; Wahab, R.A.; Lee, S.L.; Ponnusamy, V.K.; Chen, Y.-H. Current Perspectives of Metal-Based Nanomaterials as Photocatalytic Antimicrobial Agents and Their Therapeutic Modes of Action: A Review. *Environ. Res.* **2023**, 115578. [[CrossRef](#)] [[PubMed](#)]
84. Shah, M.Z.; Guan, Z.-H.; Din, A.U.; Ali, A.; Rehman, A.U.; Jan, K.; Faisal, S.; Saud, S.; Adnan, M.; Wahid, F. Synthesis of Silver Nanoparticles Using Plantago Lanceolata Extract and Assessing Their Antibacterial and Antioxidant Activities. *Sci. Rep.* **2021**, *11*, 1–14. [[CrossRef](#)] [[PubMed](#)]
85. Nefedova, E.; Shkil, N.; Luna Vazquez-Gomez, R.; Garibo, D.; Pestryakov, A.; Bogdanchikova, N. AgNPs Targeting the Drug Resistance Problem of *Staphylococcus aureus*: Susceptibility to Antibiotics and Efflux Effect. *Pharmaceutics* **2022**, *14*, 763. [[CrossRef](#)] [[PubMed](#)]
86. Molleman, B.; Hiemstra, T. Time, PH, and Size Dependency of Silver Nanoparticle Dissolution: The Road to Equilibrium. *Environ. Sci. Nano* **2017**, *4*, 1314–1327. [[CrossRef](#)]
87. Mateo, E.M.; Jiménez, M. Silver Nanoparticle-Based Therapy: Can It Be Useful to Combat Multi-Drug Resistant Bacteria? *Antibiotics* **2022**, *11*, 1205. [[CrossRef](#)]
88. Canaparo, R.; Foglietta, F.; Limongi, T.; Serpe, L. Biomedical Applications of Reactive Oxygen Species Generation by Metal Nanoparticles. *Materials* **2020**, *14*, 53. [[CrossRef](#)]
89. Dakal, T.C.; Kumar, A.; Majumdar, R.S.; Yadav, V. Mechanistic Basis of Antimicrobial Actions of Silver Nanoparticles. *Front. Microbiol.* **2016**, *7*, 1831. [[CrossRef](#)]
90. Musimun, C.; Papiernik, D.; Permpoonpattana, P.; Chumkaew, P.; Srisawat, T. Synergy of Green-Synthesized Silver Nanoparticles and Vatica Diospyroides Fruit Extract in Inhibiting Gram-Positive Bacteria by Inducing Membrane and Intracellular Disruption. *J. Exp. Nanosci.* **2022**, *17*, 420–438. [[CrossRef](#)]
91. Sawpari, R.; Samanta, S.; Banerjee, J.; Das, S.; Dash, S.S.; Ahmed, R.; Giri, B.; Dash, S.K. Recent Advances and Futuristic Potentials of Nano-Tailored Doxorubicin for Prostate Cancer Therapy. *J. Drug Deliv. Sci. Technol.* **2023**, *81*, 104212. [[CrossRef](#)]
92. Yin, I.X.; Zhang, J.; Zhao, I.S.; Mei, M.L.; Li, Q.; Chu, C.H. The Antibacterial Mechanism of Silver Nanoparticles and Its Application in Dentistry. *Int. J. Nanomed.* **2020**, *15*, 2555–2562. [[CrossRef](#)]
93. Gold, K.; Slay, B.; Knackstedt, M.; Gaharwar, A.K. Antimicrobial Activity of Metal and Metal-Oxide Based Nanoparticles. *Adv. Ther.* **2018**, *1*, 1700033. [[CrossRef](#)]
94. Qayyum, S.; Oves, M.; Khan, A.U. Obliteration of Bacterial Growth and Biofilm through ROS Generation by Facilely Synthesized Green Silver Nanoparticles. *PLoS ONE* **2017**, *12*, e0181363. [[CrossRef](#)]
95. Lewis, J.S., II; Bush, K. Antibacterial Agents. In *Manual of Clinical Microbiology*; John Wiley & Sons, Ltd.: New York, NY, USA, 2015; pp. 1169–1211. ISBN 978-1-68367-280-7.
96. Lin, J.; Zhou, D.; Steitz, T.A.; Polikanov, Y.S.; Gagnon, M.G. Ribosome-Targeting Antibiotics: Modes of Action, Mechanisms of Resistance, and Implications for Drug Design. *Annu. Rev. Biochem.* **2018**, *87*, 451–478. [[CrossRef](#)]

97. Chellat, M.F.; Raguž, L.; Riedl, R. Targeting Antibiotic Resistance. *Angew. Chem. Int. Ed.* **2016**, *55*, 6600–6626. [[CrossRef](#)]
98. Leach, K.L.; Brickner, S.J.; Noe, M.C.; Miller, P.F. Linezolid, the First Oxazolidinone Antibacterial Agent. *Ann. N. Y. Acad. Sci.* **2011**, *1222*, 49–54. [[CrossRef](#)]
99. Crowley, P.D.; Gallagher, H.C. Clotrimazole as a Pharmaceutical: Past, Present and Future. *J. Appl. Microbiol.* **2014**, *117*, 611–617. [[CrossRef](#)]
100. Afkhami, F.; Forghan, P.; Gutmann, J.L.; Kishen, A. Silver Nanoparticles and Their Therapeutic Applications in Endodontics: A Narrative Review. *Pharmaceutics* **2023**, *15*, 715. [[CrossRef](#)]

**Disclaimer/Publisher’s Note:** The statements, opinions and data contained in all publications are solely those of the individual author(s) and contributor(s) and not of MDPI and/or the editor(s). MDPI and/or the editor(s) disclaim responsibility for any injury to people or property resulting from any ideas, methods, instructions or products referred to in the content.